Superior high-temperature resistance of aluminium nitride particle-reinforced aluminium compared to silicon carbide or alumina particle-reinforced aluminium

SHY-WEN LAI AND D. D. L. CHUNG
Composite Materials Research Laboratory, Furnas Hall, State University of New York at Buffalo, Buffalo, NY 14260, USA

Aluminium–matrix composites containing AlN, SiC or Al_2O_3 particles were fabricated by vacuum infiltration of liquid aluminium into a porous particulate preform under an argon pressure of up to 41 MPa. Al/AlN had similar tensile strengths and higher ductility compared to Al/SiC of similar reinforcement volume fractions at room temperature, but exhibited higher tensile strength and higher ductility at 300–400 °C and at room temperature after heating at 600 °C for 10–20 days. The ductility of Al/AlN increased with increasing temperature from 22–400 °C, while that of Al/SiC did not change with temperature. At 400 °C, Al/AlN exhibited mainly ductile fracture, whereas Al/SiC exhibited brittle fracture due to particle decohesion. Moreover, Al/AlN exhibited greater resistance to compressive deformation at 525 °C than Al/SiC. The superior high-temperature resistance of Al/AlN is attributed to the lack of a reaction between aluminium and AlN, in contrast to the reaction between aluminium and SiC in Al/SiC. By using Al–20Si–5Mg rather than aluminium as the matrix, the reaction between aluminium and SiC was arrested, resulting in no change in the tensile properties after heating at 500 °C for 20 days. However, the use of Al–20Si–5Mg instead of aluminium as the matrix caused the strength and ductility to decrease by 30% and 70%, respectively, due to the brittleness of Al–20Si–5Mg. Therefore, the use of AlN instead of SiC as the reinforcement is a better way to avoid the filler–matrix reaction. Al/Al_2O_3 had lower room-temperature tensile strength and ductility compared to both Al/AlN and Al/SiC of similar reinforcement volume fractions, both before and after heating at 600 °C for 10–20 days. Al/Al_2O_3 exhibited brittle fracture even at room temperature, due to incomplete infiltration resulting from Al_2O_3 particle clustering.

1. Introduction

Aluminium is attractive compared to many other metals (e.g. copper, tungsten, etc.) because of its combination of a low density and a high thermal conductivity. However, it has the disadvantage of a high coefficient of thermal expansion (CTE) compared to many other metals (e.g. copper, tungsten, etc.). A low CTE and a high thermal conductivity are desirable for applications as electronic heat sinks and space structures. In addition, a low density is desirable for aerospace electronics and space structures. An effective way for lowering the CTE is the addition of a low CTE filler to form a metal–matrix composite. Thus, an aluminimum–matrix composite exhibits (i) a low CTE, (ii) in the case of a filler which is thermally conductive, a high thermal conductivity, and (iii) in the case of a filler of low density, a low density as well. Hence, the ideal filler has a low CTE, a low density and a high thermal conductivity.

The choice of the filler is also governed by the reactivity between the filler and the matrix, as ex-

cessive reaction damages the filler and weakens the bonding between the filler and the matrix, though limited reaction helps the adhesion between them. The reaction, if present, becomes more severe as the temperature increases. Thus, a reaction is not desirable for the high-temperature resistance of the composite. High-temperature resistance is desirable for applications in fusion welding and electronic heat sinks.

The high-temperature resistance of aluminium–matrix composites containing silicon carbide (SiC) particles (the most widely used reinforcement for aluminium) is limited by the reaction between aluminium and SiC, as this reaction forms Al_4C_3 and silicon and weakens the interface between the filler and the matrix when the reaction becomes excessive. Alternative reinforcements which do not react with aluminium include alumina (Al_2O_3) and aluminium nitride (AlN). Alumina particles can be considered the second most widely used reinforcement for aluminium, but little work [1, 2] has been reported on aluminium reinforced by AlN, which has an additional advantage of a

TABLE I Properties of AlN, SiC and Al_2O_3 powder

	AlN	SiC	Al_2O_3
Mean particle size (μm)	3.7	3.0	3.0–3.5
Specific surface area ($m^2 g^{-1}$)	2.5–4.0	–	3
Density ($g cm^{-3}$)	3.26	3.18	3.97
Young's modulus (GPa)	345[a]	400–440	379[a]
Electrical resistivity (Ω cm)	$\geq 10^{13}$	–	$\geq 10^{14}$
Dielectric constant	8.2–9.0	–	9.3
Thermal conductivity ($W m^{-1} K^{-1}$)	160–220	90	20
Coefficient of thermal expansion (μm $m^{-1} °C^{-1}$)	3.3[a]	3.4[a]	7.0[a]
Crystal structure	Hexagonal	Hexagonal	Corundum

[a] From [1].

high thermal conductivity compared to both SiC and Al_2O_3. The properties of AlN, SiC and Al_2O_3 are shown in Table I.

This work is focused on Al/AlN particulate composites, with emphasis on the high-temperature resistance and mechanical properties compared to Al/SiC and Al/Al_2O_3.

Al/AlN particulate composites had been previously studied by Geiger [1, 2], who measured the room-temperature properties of composites made by powder metallurgy and subsequent extrusion. Such composites had also been made by Aghajanian et al. by liquid-metal infiltration in a controlled atmosphere furnace [3]. Melt infiltration was also used by Toy and Scott [4] to produce Al/sintered AlN composites. In this paper, we report the high-temperature properties of Al/AlN.

The elevated temperature tensile properties of various discontinuously reinforced aluminium alloys, such as 6061 [5, 6], 2024 [7], 2124 [8–11], 7075 [12], 1100 [9, 13], 336 [14] and 332 [15] have been reported. The reinforcement was alumina (particles) or SiC (whiskers or particles) and the volume fraction ranged from 15% to 30%. Generally, composites fabricated by powder metallurgy or extrusion methods provided a higher tensile strength than those made by casting techniques. In most cases, the tensile strength of the composites upon heating started to drop sharply at 300 °C and converged to about 70 MPa at 400 °C, even though the room-temperature tensile strengths of different composites were very different. An exception is in the case of $2124/SiC_p$ (20 wt % SiC), which exhibited a tensile strength of about 120 MPa at 400° [10]. No information on the elevated temperature properties of Al/SiC containing > 30 vol% SiC or Al/AlN of any AlN volume fraction has been reported.

It is of interest to evaluate the elevated temperature mechanical properties of Al/SiC, Al/AlN and Al/Al_2O_3 with high volume fractions and to investigate the effect of the filler species on the elevated temperature mechanical properties and on the room-temperature properties after heating.

2. Experimental procedure
2.1. Composite fabrication
The AlN (AlNel Grade A-100) and SiC (1200-W) particles used were kindly provided by Advanced
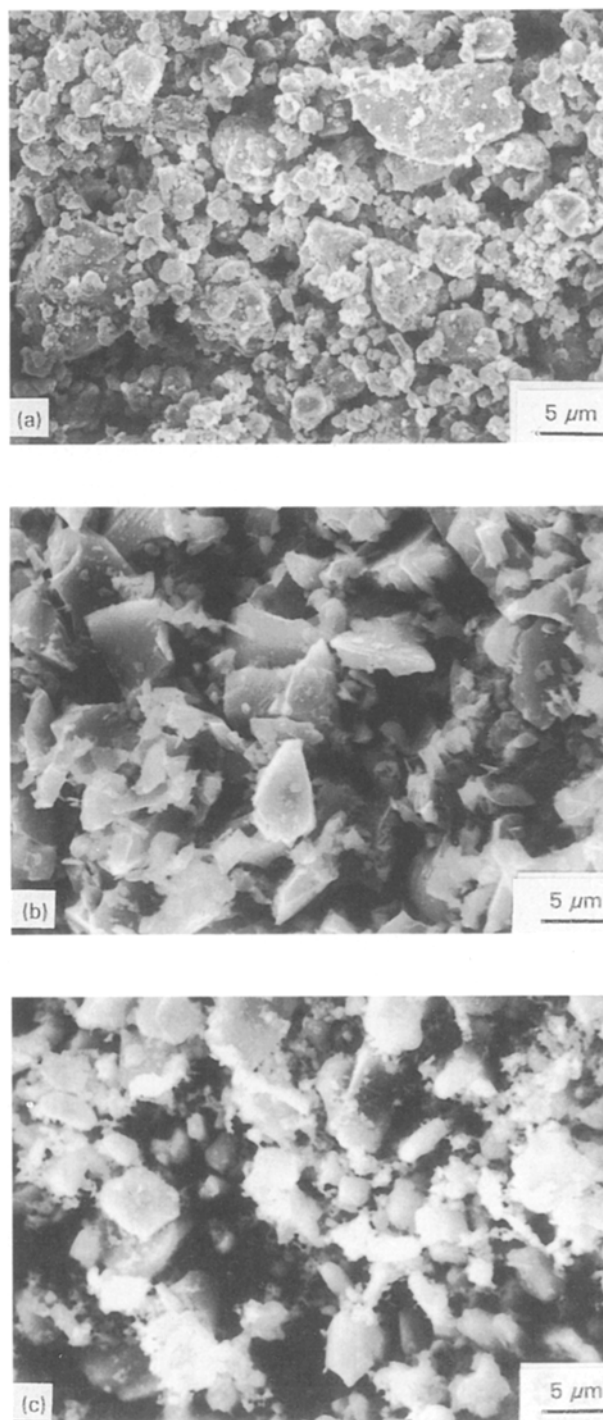

Figure 1 Scanning electron micrographs of AlN, SiC and Al_2O_3 powders.

Refractory Technologies, Inc. and Electro Abrasives, Inc., respectively. The calcined alumina particles (A-17) were obtained from the Aluminium Company of America (ALCOA). The AlN particle size ranged from 2 to 7 µm, with a mean at 3.7 µm, but coarse particles of up to 12 µm were also present in the powders. The SiC particle size ranged from 1–10 µm, with a mean at 3 µm. The alumina particle size had an average of 3.0–3.5 µm. The properties of the three kinds of powders are listed in Table I. The composition of AlN was 66.0% Al, 33.0% N, 0.07% C, 1.0% O, 0.005% Fe and 0.005% Si. The composition of SiC was 98.5% SiC, 0.5% SiO_2, 0.3% Si, 0.08% Fe, 0.1% Al, 0.3% C. The calcined alumina contained 99.7% Al_2O_3, 0.08% Na_2O, 0.02% SiO_2, 0.01% Fe_2O_3 and 0.001% B_2O_3.

Fig. 1 shows scanning electron micrographs of AlN, SiC and calcined Al_2O_3 powders (without any binder). Both AlN and SiC had "clean" particle surfaces. However, the calcined Al_2O_3 had very fine particles surrounding each Al_2O_3 particle, so that particle clustering occurs and results in little space for the liquid-metal infiltration. No particle clustering was found in the AlN and SiC powders.

The metal used, unless stated otherwise, was aluminium (170.1), the tensile strength of which was 65 MPa. Its composition was Al (99.77%), Fe (0.16%) and Si (0.07%) and the melting temperature was 660 °C. Other alloys used were 6061 (Mg(1.05%), Si(0.6%), Mn(0.28%), Cr(0.2%)), 413.1 (Si(12.0%), Fe(1.3%), Cu(1.0%), Mg(0.1%)), Al–20Si–5Mg and Al–5Mg. The last two alloys were made from aluminium (170.1). Magnesium is known to improve the wetting between the ceramic reinforcement and the matrix [16, 17]. Silicon added to the alloy is known to prevent reaction of SiC with the aluminium melt during fabrication and to reduce the CTE of the composite. The CTE of silicon is only $4 \times 10^{-6}\,°C^{-1}$, as compared to $25 \times 10^{-6}\,°C^{-1}$ for pure aluminium.

The metal–matrix composites were fabricated by vacuum infiltration of a liquid metal into a porous perform under an argon pressure. The preform was a green body comprising AlN, SiC or Al_2O_3 powder. During composite fabrication, the preform was placed at the bottom of a steel mould (Fig. 2). Above the preform was placed an aluminium ingot. The mould chamber was evacuated using a mechanical pump (A0–A1 in Fig. 3). Then the chamber was heated to 800 °C (A1–A2 in Fig. 3). The temperature was maintained for a period of time to ensure that the alloy melted completely and that the temperature of any part of the chamber was approximately equal (A2–A3 in Fig. 3). Then the temperature was allowed to drop at a rate of 3.0–10.0 °C min^{-1} to the liquidus temperature, T_1, or near the liquidus temperature, in this case 670 °C (A3–A4 in Fig. 3). When the temperature just started to drop from 800 °C, the argon gas pressure started to be increased from 0 p.s.i. up to a maximum of, unless stated otherwise, 6000 p.s.i. (41 MPa) for pure aluminium or 3500 p.s.i. (24 MPa) for Al–5Mg. This pressure was applied to the surface of the melt to force the melt to penetrate the porous preform completely (A4–A5 in Fig. 3). Then the chamber was cooled with the help of a cooling water jacket outside
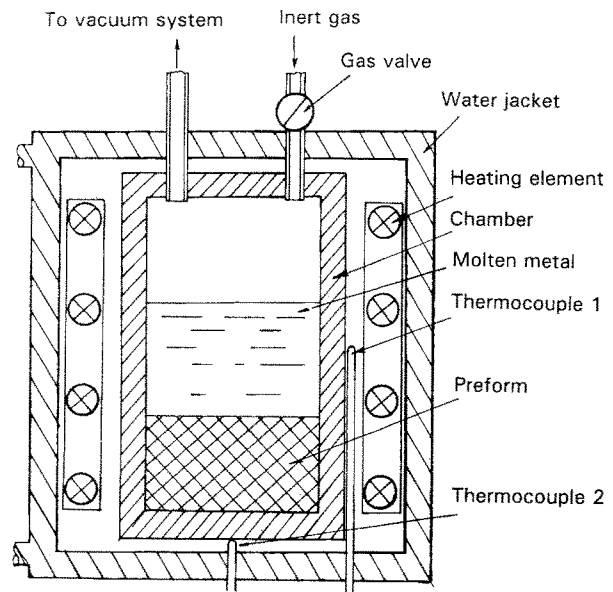
Figure 2 Schematic illustration of the steel mould for making metal–matrix composites by vacuum infiltration of a liquid metal under an inert gas pressure.
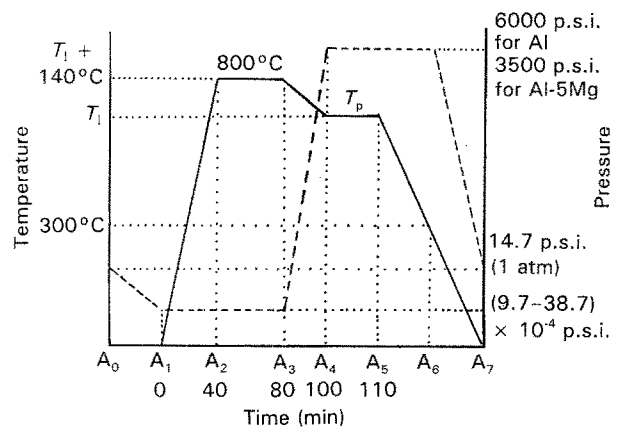
Figure 3 Variation of the temperature and pressure in the process of making metal–matrix composites by liquid-metal infiltration.

the chamber (A5–A6 in Fig. 3). When the temperature was 300 °C, the pressure started to be released (A6–A7 in Fig. 3).

The AlN, SiC or Al_2O_3 preforms were prepared by wet casting, which involved compressing in a die a slurry containing AlN, SiC or Al_2O_3 powder, a liquid carrier (acetone) and a binder (a phosphate [18–20]). (A silica colloid had also been used as the binder, but it resulted in preforms that were much weaker than those obtained with a phosphate binder.) Acetone was used because it is non-aqueous and AlN reacts with H_2O to form $Al(OH)_3$ and NH_3. The carrier/binder ratio was from 40:1 to 45:1 by volume, as this amount of binder was sufficient to maintain rigidity in the preform. The resulting dry preform contained ~ 0.1 wt % binder. Excessive amounts of binder caused the preform to be not porous enough for subsequent liquid-metal infiltration even at 6000 p.s.i. (41 MPa). The die allowed excessive liquid to be squeezed out. After removal from the die, the compact was dried in a fume hood at room temperature for 3 h. After drying, which removed most of the acetone, the

preform was fired by (i) placing the preform in a furnace at room temperature, (ii) heating to 510 °C at a controlled rate of 1.4 °C min^{-1}, (iii) holding at 510 °C for 3 h, and (iv) cooling in the closed furnace. Excessive heating and a non-uniform temperature distribution in the furnace had to be avoided, because they would cause quick evolution of acetone and thermal stresses, thus resulting in cracking during the firing. No oxidation of AlN was detected with X-ray diffraction from the AlN preforms after baking in air at 660 °C for 43 h. For the sake of comparison, a mixture of AlN with 1 wt % Al_2O_3 was tested as a reference, showing clear Al_2O_3 diffraction peaks. SiC preforms baked at 510 °C for 8 h gave the same X-ray diffraction peaks as the plain SiC powder.

The pressure used during compression of the slurry was adjusted to vary the AlN, SiC or Al_2O_3 volume fraction in the resulting preform, although the range of volume fraction achieved was quite narrow, as shown in Table II for the AlN compact. The minimum AlN volume fraction achieved with this method was 55%.

The preforms were cylinders, 4.00 cm diameter, with a height-to-diameter ratio of 0.3–0.5. Fig. 4 shows scanning electron micrograph of an AlN preform. No binder was observed distinctly.

Although all the work described in this paper involved preforms prepared by the wet-forming technique, the dry powder compact method was tried and resulted in preforms that were fragile and non-uniform in the reinforcement distribution. In this paper, "composite cylinder" refers to the metal-infiltrated cylindrical preform.

TABLE II Effect of applied pressure (during slurry compression) on the AlN volume fraction of the resulting preform

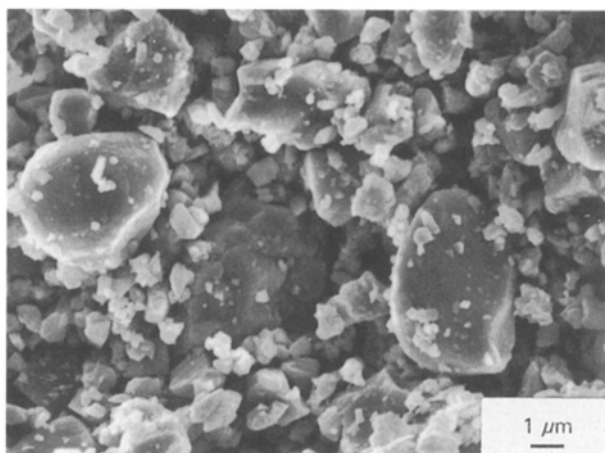| Applied pressure (MPa)	AlN (vol %)
0	55
7.8	58–59
2 × 7.8	60.5
3 × 7.8	61.5
4 × 7.8	62.3
5 × 7.8	65.3

Figure 4 Scanning electron micrograph of an AlN preform with a uniform distribution of AlN particles. No binder was observed distinctly.

2.2. Composite characterization
2.2.1. Metallography
Fig. 5 shows optical micrographs of polished (not etched) sections of AlN composites prepared at infiltration pressures of 3500 p.s.i. (24 MPa), 4500 p.s.i. (31 MPa) and 6000 p.s.i. (41 MPa). The porosity decreased with increasing pressure; it was 12.4% at 3500 p.s.i. (Fig. 5a), 5.4% at 4500 p.s.i. (Fig. 5b), and was 1.1%–1.4% at 6000 p.s.i. (Fig. 5c) for a composite containing 58.6 vol% AlN. Fig. 5c for 6000 p.s.i. represents one of the most thoroughly infiltrated composites in this work. A higher magnification SEM image of a similar composite containing 62.5% AlN is shown in Fig. 6; the porosity was 0.5%.
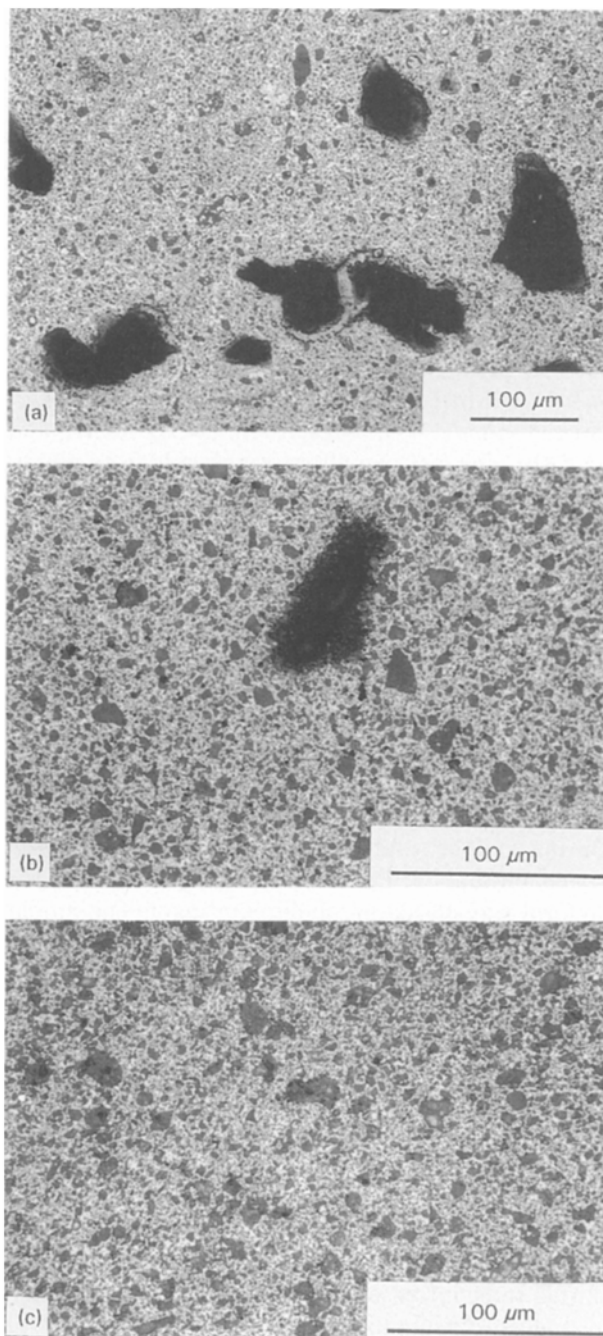

Figure 5 Optical micrographs (after mechanical polishing, without etching) of Al/AlN fabricated at an infiltration pressure of (a) 3500 p.s.i. (24 MPa), (b) 4500 p.s.i. (31 MPa) and (c) 6000 p.s.i. (41 MPa). The porosity decreased with increasing infiltration pressure.
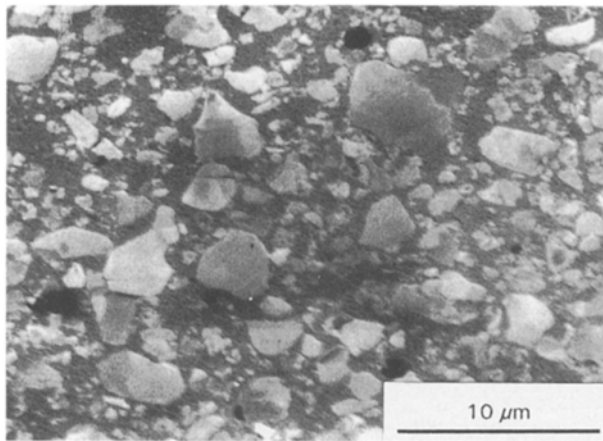
Figure 6 Scanning electron micrograph of Al/AlN (62.5 vol %) fabricated at an infiltration pressure of 6000 p.s.i. (41 MPa). The porosity was 0.5%.
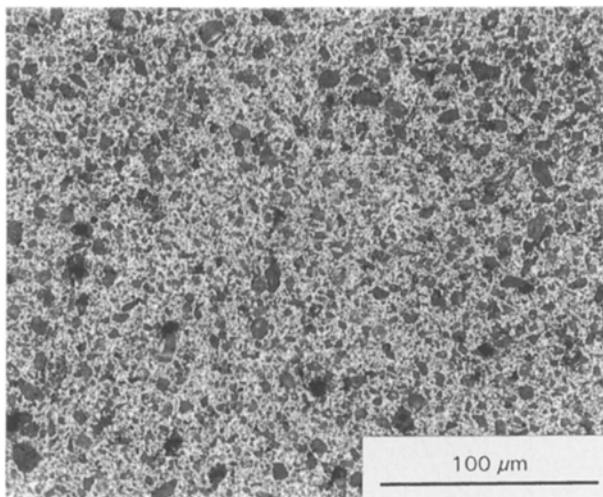

Figure 7 Optical micrographs (after mechanical polishing, without etching) of Al–5Mg/AlN fabricated at an infiltration pressure of 3500 p.s.i. (24 MPa).

Figure 8 (a) Scanning electron micrograph of Al/Al$_2$O$_3$ (61.4 vol % Al$_2$O$_3$). (b) Dark-field optical micrograph of the same composite.

Fig. 7 shows an optical micrograph of a polished (not etched) section of a composite containing 60 vol % AlN, made with Al–5Mg as the matrix at an infiltration pressure of 3500 p.s.i. (24 MPa). The porosity was 2.7%. Hence, magnesium in the matrix alloy enabled the required infiltration pressure to decrease to 3500 p.s.i. (24 MPa).

The Al/SiC composite fabricated at 6000 p.s.i. (41 MPa) exhibited less porosity than the Al/AlN composite fabricated at the same pressure because of the higher wettability between aluminium and the SiC due to the interfacial reaction of SiC with Al. It was reported [21] that a 52% SiC particulate compact of 9.63 μm particle size could be infiltrated with pure aluminium at 800 °C and 106 p.s.i (724 kPa). In contrast, Al/Al$_2$O$_3$ fabricated under the same condition showed more porosity than Al/AlN. Fig. 8a shows a dark-field optical micrograph of a polished (not etched) Al/Al$_2$O$_3$ (61.4 vol % Al$_2$O$_3$) composite, in which small but uniformly distributed pores were observed throughout the composite; Fig. 8b shows a scanning electron micrograph of the same sample in
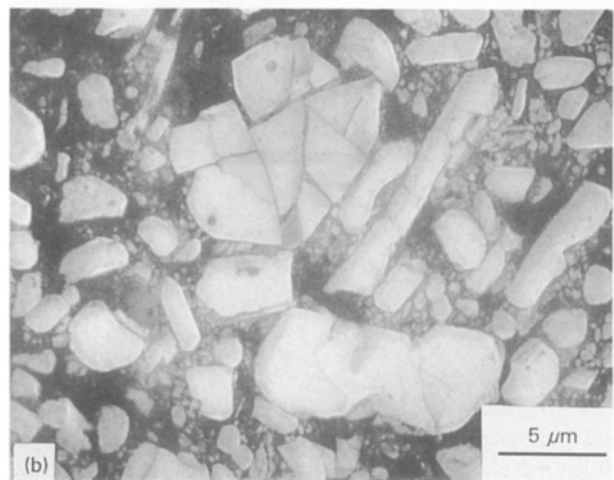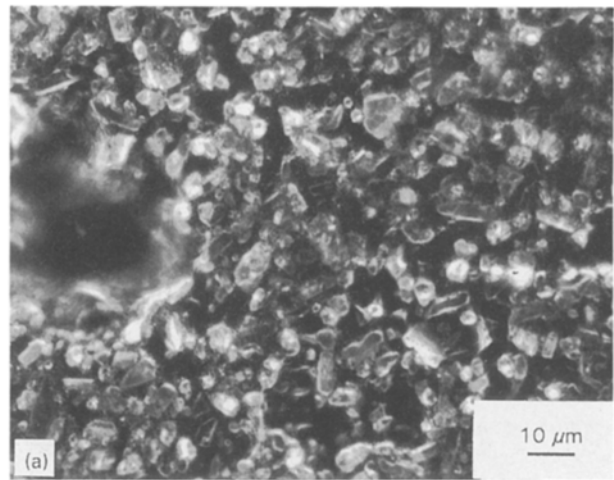
which cracks within the Al$_2$O$_3$ particles were observed, indicating a weaker particle strength for Al$_2$O$_3$; the porosity was 3%–5%.

All Al/AlN, Al/SiC and Al/Al$_2$O$_3$ composites showed a uniform distribution of particles and thus are expected to have isotropic properties.

Different microstructures (after mechanical polishing) were found between the cylindrical edge and body centre regions of an Al/SiC composite cylinder (55 vol % SiC) after infiltration and before machining, as shown in Fig. 9. The difference in microstructure is related to the more extensive interfacial reaction between aluminium and SiC in the edge region. Hence the edge region shows a lower density of SiC particles than the central region. More Al–SiC reaction occurred around the edge due to the proximity to excess aluminium and a longer metal–particle contact time during infiltration. On the other hand, as shown in Fig. 9, the edge and central regions of an Al/AlN composite cylinder (60.0 vol % AlN) show essentially no difference in microstructure.

2.2.2. Mechanical properties

Tensile testing was performed using a hydraulic mechanical testing system (MTS) with a loading rate of
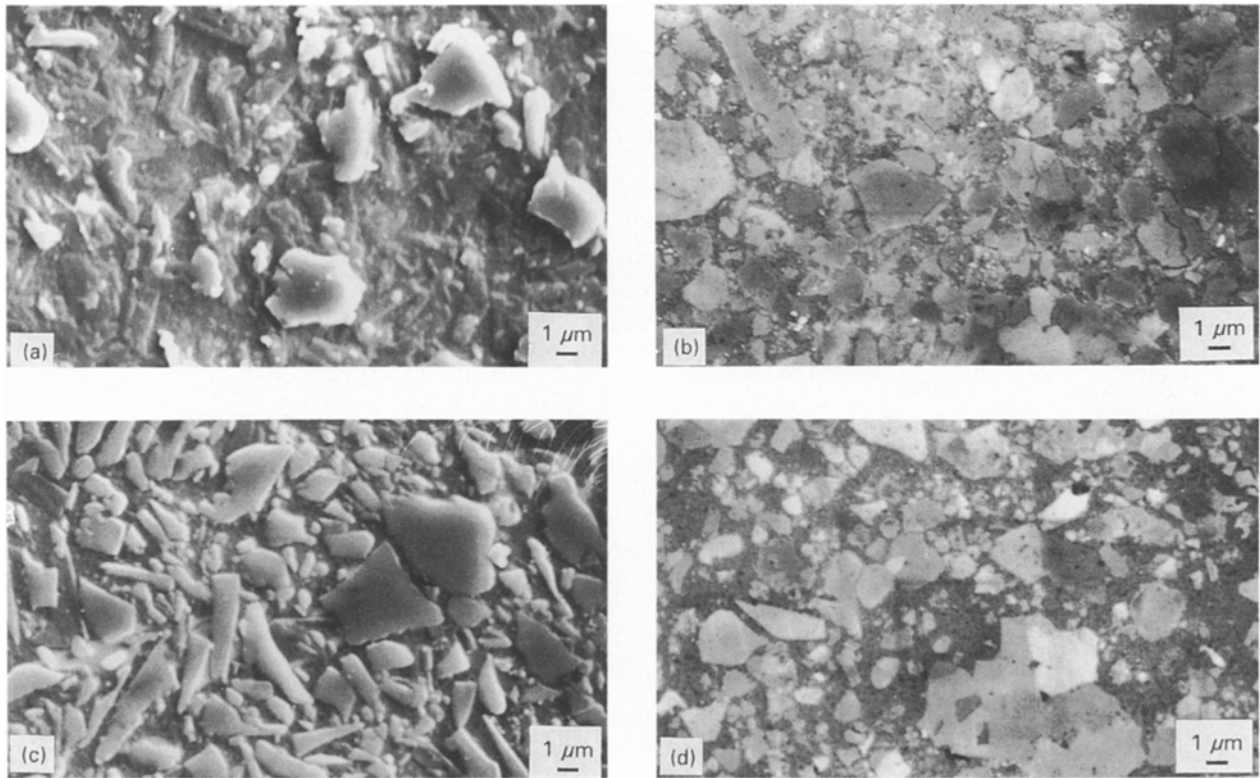
Figure 9 Scanning electron micrographs (after mechanical polishing, without etching) of a, c Al/SiC and b, d Al/AlN in the (a, b) edge and (c, d) central regions of the composite cylinders.

$120 \, \mathrm{lb \, min^{-1}}$ ($534 \, \mathrm{N \, min^{-1}}$) at both room and elevated temperatures. Each sample was in the shape of a dogbone, as shown in Fig. 10. Three to five samples of each type were tested. The Young's modulus was measured using a strain gauge at low loads. The ductility was determined by drawing two parallel lines marking the gauge length on the sample and measuring the distance between the lines before and after the tensile test using calipers.

High-temperature tensile testing was performed using the same method, except that a resistance furnace was placed around the sample. The temperature accuracy was $\pm 10 \, ^\circ\mathrm{C}$. Each specimen was held in the furnace at the test temperature for 30 min prior to testing.

Typical stress–strain curves of Al/AlN, Al/SiC, Al/Al$_2$O$_3$ and pure aluminium are shown in Fig. 11. In contrast to the ductile aluminium matrix, all Al/AlN,
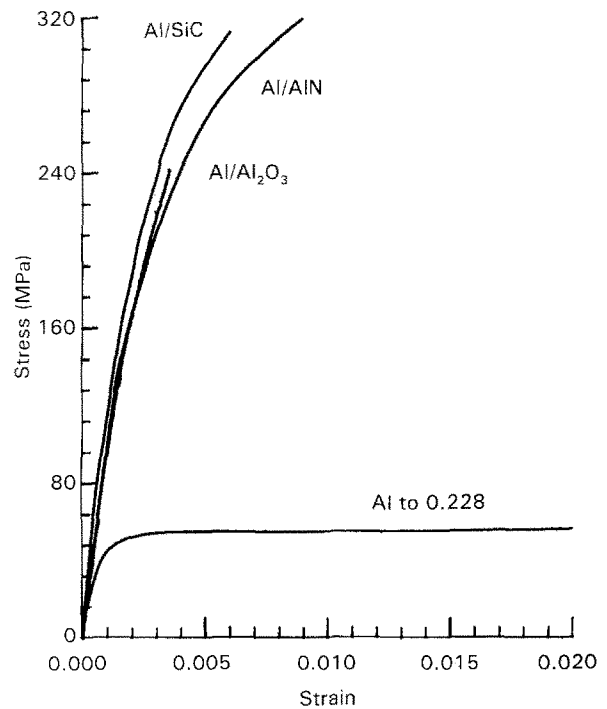

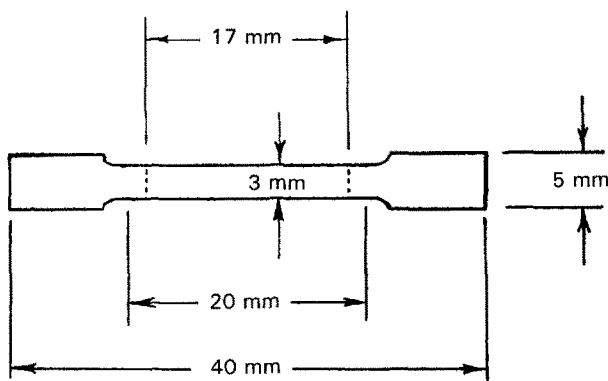*Figure 11* Typical stress–strain curves of Al/AlN, Al/SiC and pure aluminium.

Figure 10 Dimensions of a dogbone shape tensile specimen. The dashed lines indicate the gauge length markings on the specimens.

Al/SiC and Al/Al$_2$O$_3$ composites exhibited failure strains less than 1.0%. Table III shows the tensile properties at room temperature of Al/AlN, Al/SiC and Al/Al$_2$O$_3$ composites. The strength and modulus were much increased and the ductility much decreased by the addition of AlN, SiC or Al$_2$O$_3$. Al/AlN and Al/SiC of similar reinforcement volume fractions (rows 2 and

TABLE III The room-temperature tensile properties[a] of Al/AlN, Al/SiC and Al/Al$_2$O$_3$ composites

Vol. fraction	Strength (MPa)	Modulus (GPa)		Ductility (%)
		Measured	Theoretical[b]	
0	72.7 (1.1)	61.7 (3.4)	–	22.8 (1.9)
55.0% SiC	313.0 (37.5)	183.4 (15.0)	158.5	0.7 (0.3)
58.6% AlN	300.9 (25.2)	144.3 (4.2)	146.7	1.1 (0.4)
63.3% AlN	406.3 (33.9)	163.5 (36.5)	159.4	1.0 (0.2)
61.2% Al$_2$O$_3$	275.8 (14.6)	161.6 (6.9)	158.9	0.5 (0.1)
70.2% Al$_2$O$_3$	237.8 (8.4)	181.4 (10.8)	187.8	0.4 (0.1)

[a] Standard deviation shown in parentheses.
[b] Hashin and Shtrikman [22].
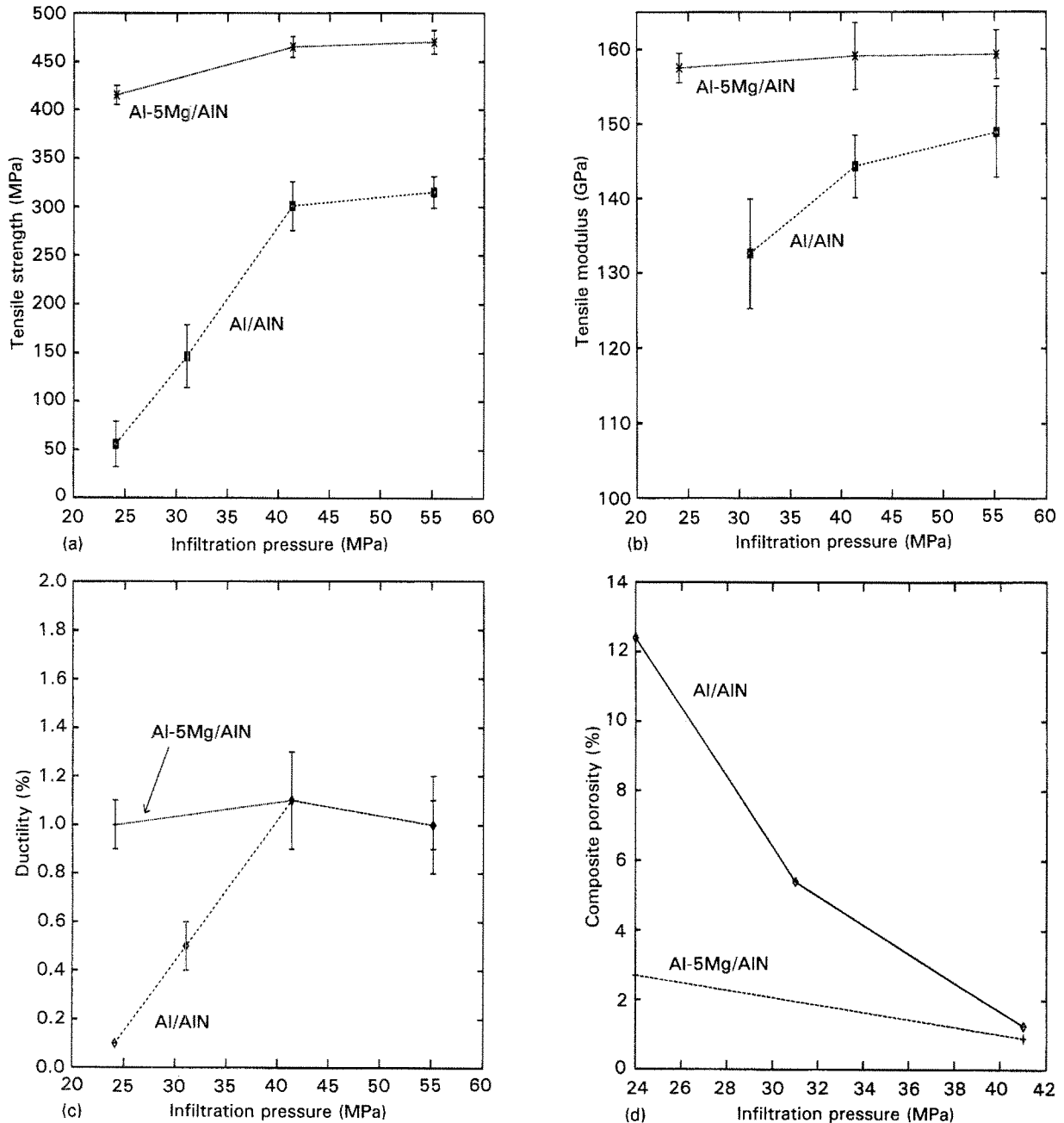$E_{AlN} = 345$ GPa, $E_{SiC} = 440$ GPa, $E_{Al_2O_3} = 379$ GPa.

Figure 12 Tensile properties and porosity of Al/AlN (59–60 vol % AlN) and Al–5Mg/AlN (60 vol% AlN) as a function of the infiltration pressure. (a) Tensile strength, (b) modulus, (c) ductility, (d) porosity.

3 of Table III) exhibited similar tensile strengths and slightly higher ductility for Al/AlN, while Al/AlN and Al/Al$_2$O$_3$ of similar reinforcement volume fractions (rows 4 and 5 of Table III) showed much higher strength and ductility for Al/AlN than Al/Al$_2$O$_3$. For Al/AlN and Al/Al$_2$O$_3$, the measured modulus and that calculated using the model of Hashin and Shtrikman (H–S) [22] agree with each other very well, but

Al/SiC had a measured modulus which was larger than the theoretical value based on this model. The high measured modulus of Al/SiC may be ascribed to the large aspect ratio (>3 based on Fig. 9) of the SiC particles – a factor which was not considered in the H–S model.

Fig. 12 shows the tensile properties and porosity of Al/AlN (59–60 vol% AlN) fabricated at infiltration pressures of 3500 p.s.i. (24 MPa), 4500 p.s.i. (31 MPa), 6000 p.s.i. (41 MPa) and 8000 p.s.i. (55 MPa). The modulus, strength and ductility of Al/AlN increased with increasing infiltration pressure up to 6000 p.s.i. (41 MPa) and remained essentially unchanged upon further increase in pressure. Note that the strength and ductility of Al/AlN increased quite linearly with increasing infiltration pressure up to 6000 p.s.i. (41 MPa). The modulus and strength of Al/AlN fabricated at the infiltration pressure of 8000 p.s.i. (55 MPa) might be slightly increased, compared to those of Al/AlN fabricated at the infiltration pressure of 6000 p.s.i. (41 MPa). This suggests that an infiltration pressure of 6000 p.s.i. (41 MPa) is an optimum pressure for making sound Al/AlN composites. As shown in Fig. 12d, the porosity of Al/AlN composites decreased with increasing infiltration pressure, thus resulting in increasing tensile properties. The infiltration pressure of 3500 p.s.i. (24 MPa), 4500 p.s.i. (31 MPa) and 6000 p.s.i. (41 MPa) yielded composites of 12.4%, 5.4% and 1.1%–1.4% porosity, respectively.

Fig. 12 also shows the tensile properties of Al–5Mg/AlN (60.0 vol% AlN) fabricated at infiltration pressures of 3500 p.s.i. (24 MPa), 6000 p.s.i. (41 MPa) and 8000 p.s.i. (55 MPa). All pressures yielded composites exhibiting similar modulus and ductility. However, the composite fabricated at the infiltration pressure of 6000 p.s.i. (41 MPa) showed a higher strength than that at 3500 p.s.i. (24 MPa) and about the same strength as that at 8000 p.s.i. (55 MPa), indicating an optimum infiltration pressure of 6000 p.s.i. (41 MPa), as in the case of Al/AlN. The infiltration pressures of 3500 p.s.i. (24 MPa) and 6000 p.s.i. (41 MPa) yielded composites of 2.7% and 0.9% porosity, respectively.

Fig. 12d shows that the porosity of both Al/AlN and Al–5Mg/AlN decreased with increasing infiltration pressure. The porosity was much decreased with the addition of 5 wt % magnesium, which promoted the wetting between aluminium and AlN. Hence, magnesium in the matrix alloy enabled the required infiltration pressure to decrease to 3500 p.s.i. (24 MPa) essentially without sacrificing the strength, modulus or ductility, as shown by comparing the data for Al/AlN and Al–5Mg/AlN in Fig. 12a–c. In addition, Fig. 12a and b show that, at any infiltration pressure, Al–5Mg/AlN exhibited higher strength and modulus than Al/AlN.

The 6061 Al alloy and 6061/AlN composite were given the T6 heat treatment (solution treatment at 529 °C for 2 h, followed by water quenching, and then annealing at 160 °C for 18 h). As shown in Table IV, the 6061 alloy without any filler showed a large increase in strength and a large decrease in ductility after the T6 treatment. On the other hand, 6061/AlN (58.1 vol% AlN) showed a small increase in strength and a small decrease in ductility after the T6 treatment, indicating that the strengthening in the composite is mainly due to the reinforcement (which has a high volume fraction) rather than the Mg_2Si precipitates resulting from the T6 treatment. The modulus was not changed by the T6 treatment for either the 6061 alloy or the 6061/AlN composite.

The Al/AlN (62.0 vol% AlN), Al/SiC (55.0 vol% SiC) and Al/Al$_2$O$_3$ (61.4 vol% Al$_2$O$_3$) composites were heated in air at up to 600 °C for up to 480 h. The room-temperature tensile properties of the composites

TABLE IV Effect of the T6 heat treatment[a] on the tensile properties[b] of 6061 Al/AlN

		AlN (vol%)	
		0	58.1
Strength (MPa)	Without T6	136.0 (3.8)	491.1 (21.0)
	With T6	281.9 (67.2)	513.2 (18.9)
Modulus (GPa)	Without T6	70.2 (1.7)	160.4 (6.3)
	With T6	70.6 (3.1)	159.2 (9.2)
Ductility (%)	Without T6	10.5 (2.8)	1.2 (0.4)
	With T6	3.4 (1.0)	1.0 (0.2)

[a] T6: solution treatment at 529 °C for 2 h, water quench, annealed at 160 °C for 18 h.
[b] Standard deviation shown in parentheses.

TABLE V Effect of heating on the tensile properties[a] of Al/AlN (62.0 vol% AlN), Al/SiC (55.0 vol% SiC) and Al/Al$_2$O$_3$ (61.4 vol% Al$_2$O$_3$)

		As-cast	Heating temperature and time		
			300 °C, 210 h	600 °C, 240 h	600 °C, 480 h
Strength (MPa)	Al/AlN	430.3 (14.1)	422.9 (9.9)	400.9 (24.1)	386.9 (18.1)
	Al/SiC	313.0 (37.5)	–	257.2 (12.4)	231.9 (36.5)
	Al/Al$_2$O$_3$	275.8 (14.6)	–	198.6 (3.2)	139.1 (9.2)
Modulus (GPa)	Al/AlN	161.6 (0.9)	163.1 (1.5)	162.3 (0.6)	161.9 (0.6)
	Al/SiC	183.4 (15.0)	–	–	–
	Al/Al$_2$O$_3$	161.6 (6.9)	–	159.7 (10.8)	167.8 (5.7)
Ductility (%)	Al/AlN	1.3 (0.3)	1.4 (0.2)	1.1 (0.1)	1.0 (0.2)
	Al/SiC	0.7 (0.3)	–	0.5 (0.3)	0.5 (0.2)
	Al/Al$_2$O$_3$	0.5 (0.1)	–	0.2–0.3	0.1–0.2

[a] Standard deviation shown in parentheses.

before (as-cast) and after heating are shown in Table V. The modulus was not affected by the heating, at least for Al/AlN and Al/Al₂O₃. The strength of Al/AlN decreased after heating at 600 °C but essentially did not after heating at 300 °C. However, the strengths of Al/SiC and Al/Al₂O₃ decreased with increasing heating time at 600 °C. The relative strengths of Al/AlN, Al/SiC and Al/Al₂O₃ relative to the corresponding values before heating are shown in Fig. 13 as functions of the heating time at 600 °C. Among the three composites, Al/AlN exhibited the least fractional reduction in strength, followed by Al/SiC; Al/Al₂O₃ exhibited the largest fractional strength reduction due to heating. As shown in Table V, the ductility of all Al/AlN, Al/SiC and Al/Al₂O₃ decreased due to heating at 600 °C for 10 or 20 days. Al/AlN did not decrease in ductility when heated at 300 °C for 210 h. The ductility of Al/SiC was smaller than that of the Al/AlN and the ductility of Al/Al₂O₃ was smaller than that of Al/SiC under all heat-treatment conditions. The fractional decrease in ductility due to heating at 600 °C was largest for Al/Al₂O₃ and least for Al/AlN.

Table VI shows the tensile strengths of Al/AlN and Al/SiC at 22, 200, 300, and 400 °C (*not* at room
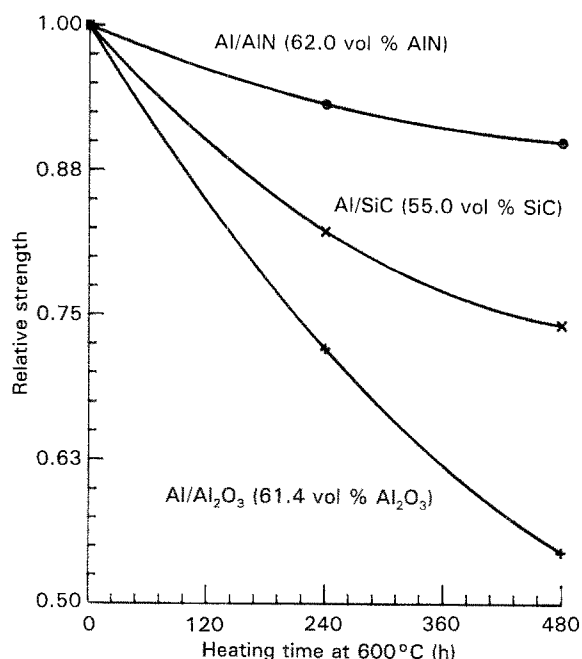
temperature after heating). The increase in temperature decreased the strength for all composites. The tensile strength of Al/AlN increased with increasing volume fraction of AlN at each test temperature. At room temperature, Al/SiC (55.0 vol % SiC) exhibited a strength similar to that of Al/AlN of a similar filler volume fraction (58.6 vol % AlN). However, at 300 and 400 °C, Al/AlN (58.6 vol % AlN) exhibited a higher tensile strength than Al/SiC (55.0 vol % SiC). Table VII shows the tensile ductility at 22, 200, 300 and 400 °C. The ductility of Al/AlN increased with increasing temperature, while that of Al/SiC essentially did not change with temperature.

The degradation of the tensile properties of Al/SiC upon heating is due to the reaction between aluminium and SiC. This reaction can be diminished by using an aluminium alloy matrix that contains silicon. Thus, the Al–20Si–5Mg alloy was used for fabricating both SiC and AlN composites. The tensile properties of the resulting composites in the as-cast state and after heating in air at 500 °C for 480 h are shown in Table VIII. A heating temperature of 500 °C was used for Al–20Si–5Mg matrix composites while a heating temperature up to 600 °C was used for aluminium matrix composites because of the lower melting temperature of Al–20Si–5Mg compared to aluminium. Table VIII shows that the tensile strength, modulus and ductility of both Al–20Si–5Mg/AlN and Al–20Si–5Mg/SiC did not change after heating at 500 °C for 480 h. This means that 20 wt % Si in the aluminium alloy matrix was sufficient to suppress the reaction between aluminium and SiC in the SiC composite. However, comparison of Tables V and VIII shows that the use of Al–20Si–5Mg instead of aluminium as the matrix resulted in a decrease of the tensile

Figure 13 Relative strength ratio of Al/AlN (62.0 vol % AlN), Al/SiC (55.0 vol % SiC) and Al/Al₂O₃ (61.4 vol % Al₂O₃) after heat treatment at 600 °C for 10 or 20 days.

TABLE VI The tensile strengths[a] of Al/AlN and Al/SiC at various temperatures

Vol fraction	Tensile strength (MPa)			
	22 °C	200 °C	300 °C	400 °C
0	72.7 (1.1)	52.8 (2.5)	25.5 (0.5)	7.3 (0.3)
55.0% SiC	313.0 (37.5)	–	209.0 (32.3)	149.5 (9.1)
58.6% AlN	300.9 (25.2)	277.7 (23.7)	266.9 (20.1)	197.5 (8.1)
63.3% AlN	406.3 (33.9)	375.8 (34.5)	312.9 (14.2)	218.9 (15.5)

[a] Standard deviation shown in parantheses.

TABLE VII The tensile ductility[a] of Al/AlN and Al/SiC composites at various temperatures

Vol fraction	Tensile ductility (%)			
	22 °C	200 °C	300 °C	400 °C
0	22.8 (1.9)	24.1 (3.8)	–	–
55.0% SiC	0.7 (0.3)	–	0.6 (0.2)	0.9 (0.3)
58.6% AlN	1.1 (0.4)	–	2.3 (0.5)	2.6 (0.3)
63.3% AlN	1.0 (0.2)	1.3 (0.3)	2.2 (0.2)	2.5 (0.4)

[a] Standard deviation shown in parantheses.

TABLE VIII Effect of heating on the tensile properties[a] of Al–20Si–5Mg/AlN (58 vol % AlN) and Al–20Si–5Mg/SiC (55 vol % SiC)

		As-cast	500 °C, 480 h
Strength (MPa)	Al–20Si–5Mg/AlN	225.4 (10.8)	225.4 (17.2)
	Al–20Si–5Mg/SiC	215.4 (20.0)	216.2 (14.1)
Modulus (GPa)	Al–20Si–5Mg/AlN	164.2 (3.7)	163.9 (2.1)
	Al–20Si–5Mg/SiC	182.5 (11.4)	184.7 (12.4)
Ductility (%)	Al–20Si–5Mg/AlN	0.2 (0.1)	0.2 (0.1)
	Al–20Si–5Mg/SiC	0.2 (0.1	0.2 (0.1)

[a] Standard deviation shown in parentheses.

strength and ductility in the as-cast state by 30% and 70%, respectively. Therefore, the use of a silicon-containing aluminium alloy matrix is not a good solution to the problem due to the reaction between aluminium and SiC. A better solution is the use of aluminium as the matrix and AlN instead of SiC as the reinforcement.

2.2.3. Fractography

Room-temperature tensile fracture surfaces are shown in Fig. 14 for Al/AlN (58.6 vol% AlN) and Al/SiC (55.0 vol% SiC). Both fracture surfaces exhibited cleavage surfaces of the filler particles and micro-dimples in the aluminium matrix, but the proportion of cleavage surfaces is lower in Al/AlN than in Al/SiC, indicating higher ductility in Al/AlN. Moreover, no particle pull-out was observed in Al/AlN, whereas particle pull-out was observed in Al/SiC, as shown by the SiC particle (~ 5 μm in size) located in the lower half of the Al/SiC photograph in Fig. 14. This indic-ates stronger bonding between aluminium and AlN than between aluminium and SiC. Note the presence of typical serratic fracture surfaces in the SiC particles in Fig. 14. The 6061/AlN and Al–5Mg/AlN com-posites exhibited similar fracture surfaces as Al/AlN. In contrast, Al/Al$_2$O$_3$ exhibited fewer but coarser microdimples and little particle cleavage (Fig. 15). Small clusters of Al$_2$O$_3$ particles were observed from the fracture surface. They are due to incomplete infilt-ration and result in a poor tensile strength. Small pores were also observed in the fracture surface.

Fig. 16 shows the fracture surfaces of Al–20Si–5Mg/AlN (57.9 vol% AlN) and Al–20Si–5Mg/SiC (55.0 vol% SiC). Both composites exhibited

Figure 15 Scanning electron micrographs of the tensile fracture surface of Al/Al$_2$O$_3$ (61.4 vol%) tested at room temperature.
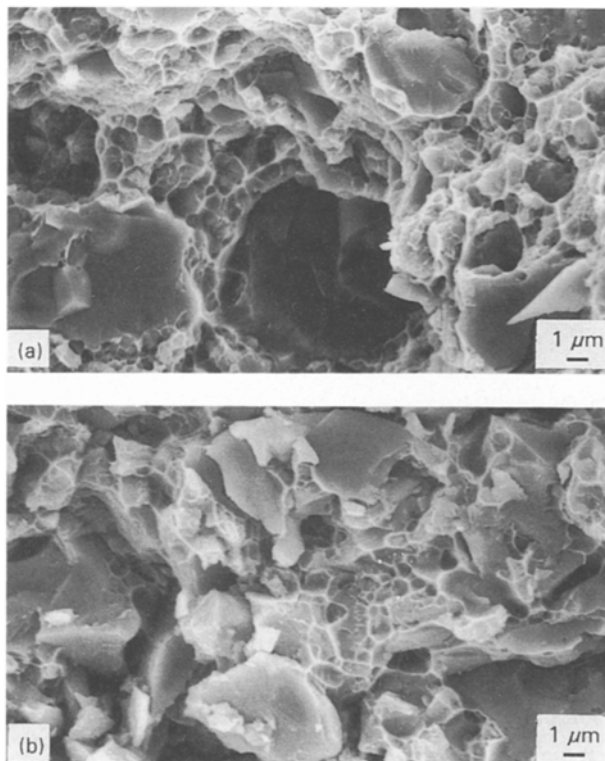

Figure 14 Scanning electron micrographs of the tensile fracture surfaces of (a) Al/AlN (58.6 vol% AlN) and (b) Al/SiC (55.0 vol% SiC) tested at room temperature.
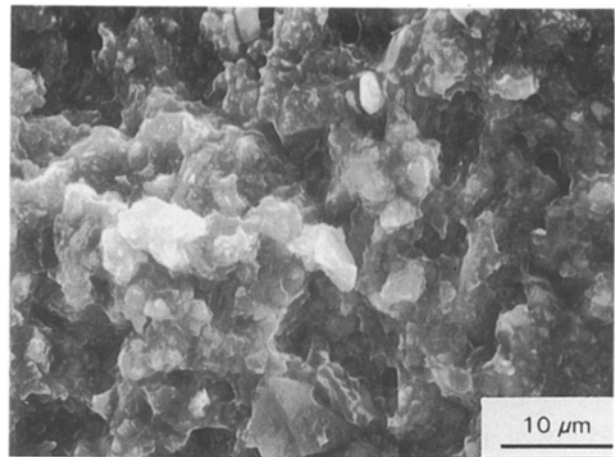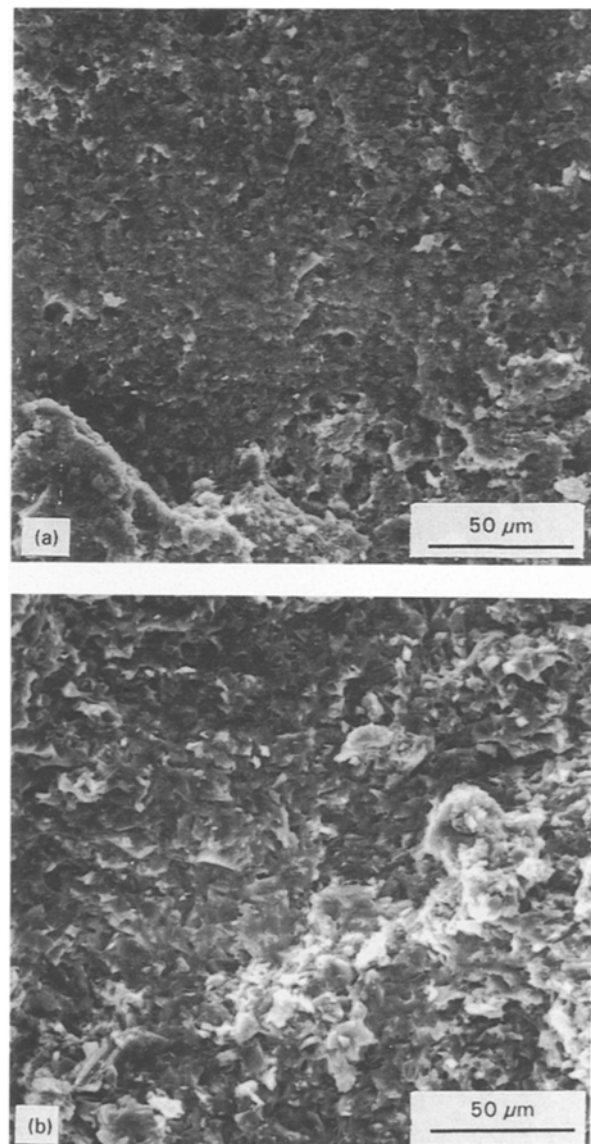

Figure 16 Scanning electron micrographs of the tensile fracture surfaces of Al–20Si–5Mg/AlN (57.9 vol% AlN) and Al–20Si–5Mg/SiC (55 vol% SiC). Both composites show a combination of completely brittle fracture regions and brittle–ductile fracture regions.

a combination of completely brittle fracture regions and brittle–ductile fracture regions. In the brittle–ductile fracture regions, as shown at a high magnification in Fig. 17, both composites had similar fracture surfaces, showing filler particle cleavage and microdimples in the matrix. No particle pull-out was found in either composite, indicating good bonding in both composites. Such a brittle–ductile fracture region was similar to that in Al/AlN or Al/SiC.

The completely brittle fracture regions in both composites were attributed to silicon precipitates and ternary Al–Si–Fe precipitates. These precipitates were as large as 300 µm. As shown in Fig. 18, no matrix microdimple was found in the completely brittle fracture regions of both composites. Cleavage existed in both matrix and particulate fillers. A crack was found in Al–20Si–5Mg/AlN to go around the AlN particles (Fig. 18a), but no such crack was found in Al/AlN (Fig. 14), indicating weaker bonding between the matrix and AlN in Al–20Si–5Mg/AlN than Al/AlN.

Figure 18 Scanning electron micrographs of Al–20Si–5Mg/AlN (57.9 vol% AlN) and Al–20Si–5Mg/SiC (55 vol% SiC) in the completely brittle fracture regions.
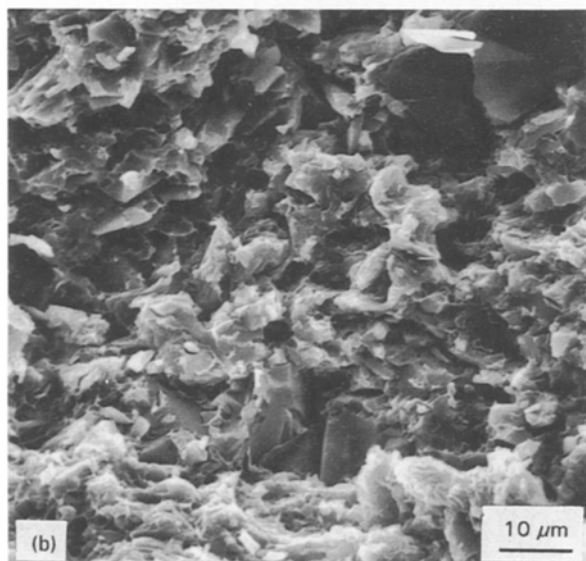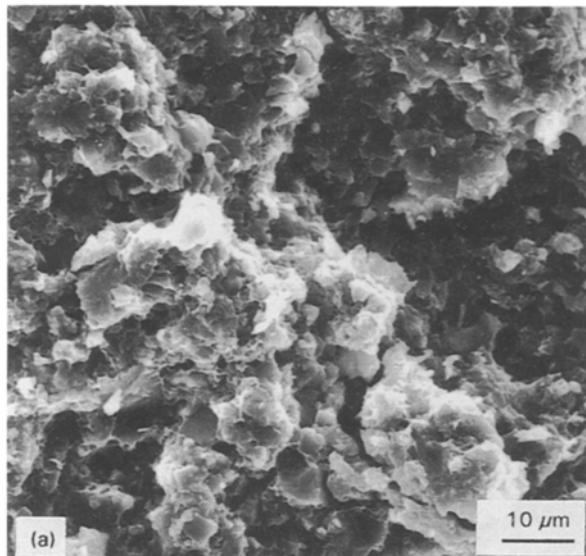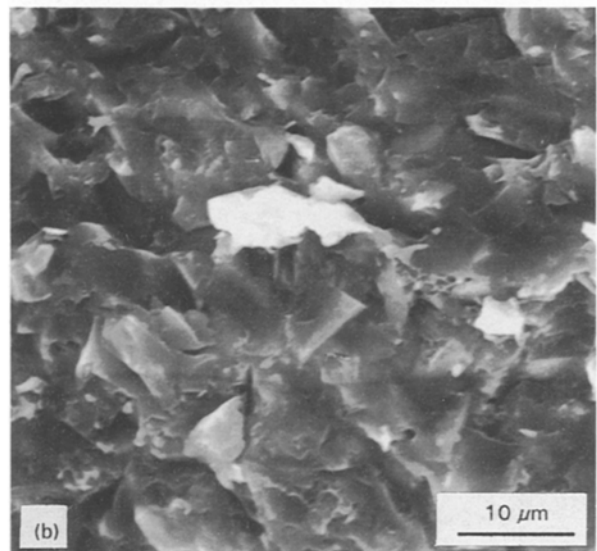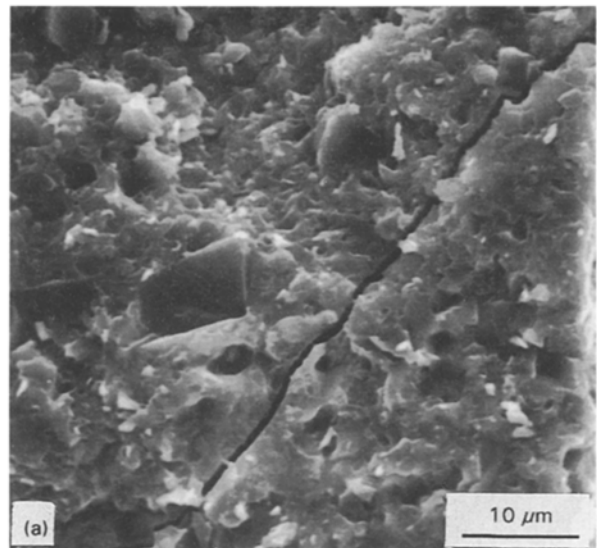

Figure 17 Scanning electron micrographs of Al–20Si–5Mg/AlN (57.9 vol% AlN) and Al–20Si–5Mg/SiC (55 vol% SiC) in the brittle–ductile fracture regions.

Both Al/AlN and Al/SiC composite specimens were cut from the infiltrated preforms to remove the excess aluminium surrounding the composite cylinder and then heated in air at 600 °C for 10 or 20 days. Al/AlN of both heat-treatment conditions (Fig. 19b and c, respectively) exhibited a combination of both ductile and brittle fracture microstructures, which are similar to those of as-cast Al/AlN (Fig. 19a). However, the size of the AlN particle cleavage facets increased with increasing heating time at 600 °C (0 days for Fig. 19a, 10 days for Fig. 19b, and 20 days for Fig. 19c). This may be ascribed to the damage of the AlN particles and interfaces due to heating. Larger ceramic particles which have more probability of having flaws are more likely to weaken because of heating. On the other hand, the Al/SiC composites that had been similarly heated exhibited hillocks (∼ 1 mm diameter and 0.5 mm high) on the composite surface, because at 600 °C the silicon-containing aluminium matrix regions melted. The silicon-containing aluminium melt migrated from the interior to the outer surfaces, as
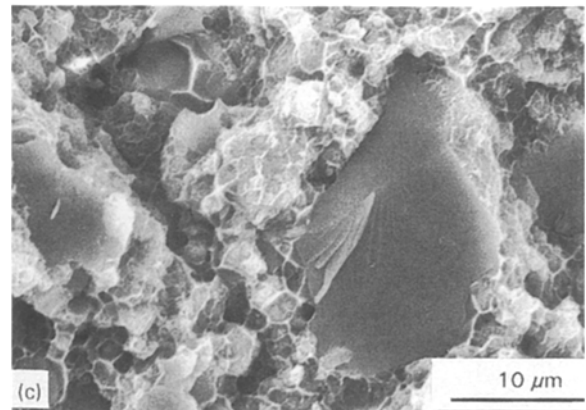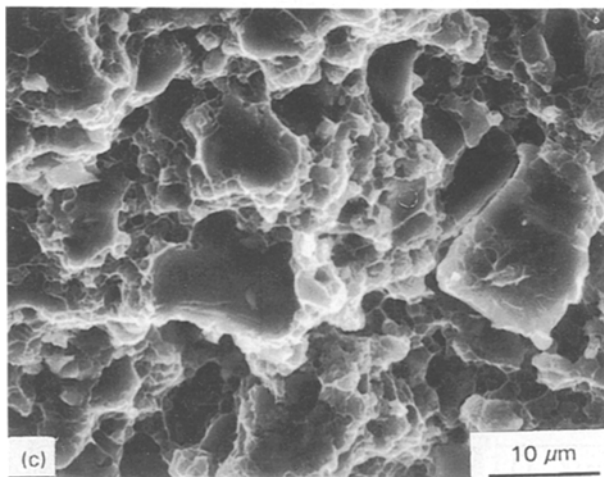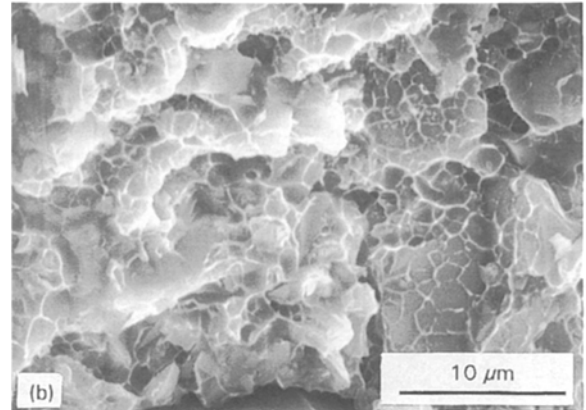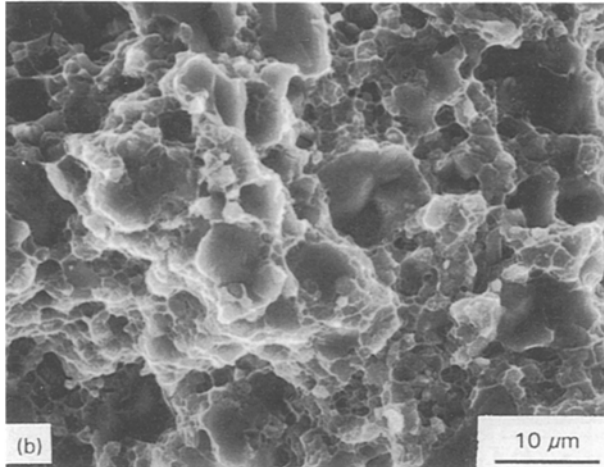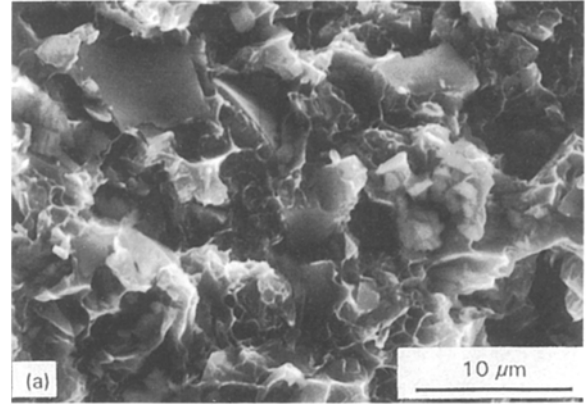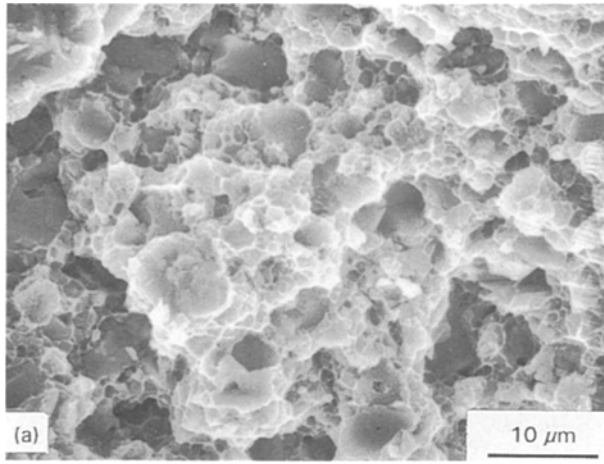
Figure 19 Scanning electron micrographs of the tensile fracture surfaces of Al/AlN (62.0 vol% AlN). (a) As-cast, (b) after heating at 600 °C for 10 days, (c) after heating at 600 °C for 20 days.

confirmed by X-ray diffraction and differential scanning calorimetry [23]. No hillock was observed on Al/AlN specimens after heating. Al/SiC of both heat-treatment conditions essentially showed the same brittle fracture microstructure compared to as-cast Al/SiC.

Fig. 20 shows the fracture surfaces of Al/AlN (58.6 vol% AlN) and Al/SiC (55 vol% SiC) at 300 and 400 °C. The fracture surfaces of both Al/AlN and Al/SiC at 300 °C (Fig. 20) are similar to those of the
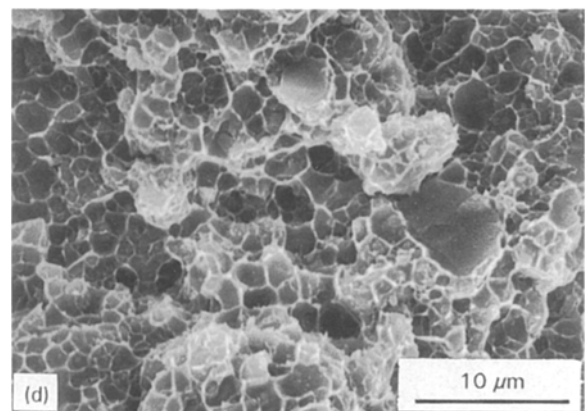
Figure 20 Scanning electron micrographs of the tensile fracture surfaces of (a, b) Al/SiC (55.0 vol% SiC) and (c, d) Al/AlN (58.6 vol% AlN) tested at elevated temperatures: (a, c) 300 °C, (b, d) 400 °C.

corresponding composite at room temperature (Fig. 14), but the fracture surfaces at 400 °C show much larger proportions of aluminium microdimples (relative to the particle cleavage surfaces) than those at 300 °C. This indicates that the matrix was much more plastic at 400 °C than at 300 °C for both composites. Compared with the fracture surfaces of Al/SiC at 300 and 400 °C, Al/AlN exhibited more matrix microdimples at each temperature, indicating larger ductility for Al/AlN. Furthermore, Al/SiC at 400 °C showed decohesion between SiC particles and the matrix (feature in the lower right portion of the photograph in Fig. 20 for Al/SiC at 400 °C, for example), again indicating weak interfacial bonding in Al/SiC.

2.2.4. Thermal expansion

The values of the coefficient of thermal expansion (CTE) of AlN, SiC, and Al_2O_3 composites were measured using a Perkin–Elmer DMA7 thermal mechanical analyser operated at a heating rate of 5 °C min^{-1} and a helium flow of 20 cm^3 min^{-1}. The temperature was scanned from 35–350 °C. Prior to the measurement, the specimens were annealed in air at 324 °C for 3 h and then furnace cooled. Three specimens of each type were tested. Fig. 21 shows the fractional expansion versus temperature curves of aluminium and Al/AlN of various AlN volume fractions in the temperature range 35–350 °C. The CTE (slope of the curve) decreased with increasing AlN volume fraction. Table IX shows the mean CTE values in various temperature ranges for the aluminium alloy matrices of 170.1, 6061, 413.1, Al–20Si–5Mg and Al–40Si–1Mg and for the AlN composites. The CTE of the matrix as well as the composites decreased with the increasing silicon content. Fig. 22 shows the CTE as a function of the silicon content for the matrix as well as the AlN and SiC composites. The CTE of the matrix decreased linearly with increasing silicon content. However, no such linearity was found in the AlN or SiC composites. The CTE of the AlN composites was slightly lower than that of SiC composites for the 170.1 matrix and more clearly for the Al–20Si–5Mg matrix. Fig. 23 shows the typical expansion curves of the matrices and of the corresponding composites containing 55 vol% AlN or SiC. Fig. 24 shows the comparison between the measured and calculated values of the mean CTE at 35–100 °C (Fig. 24a) and 35–350 °C (Fig. 24b) for the matrices 170.1 and 6061. At 35–100 °C, the measured values were close to the
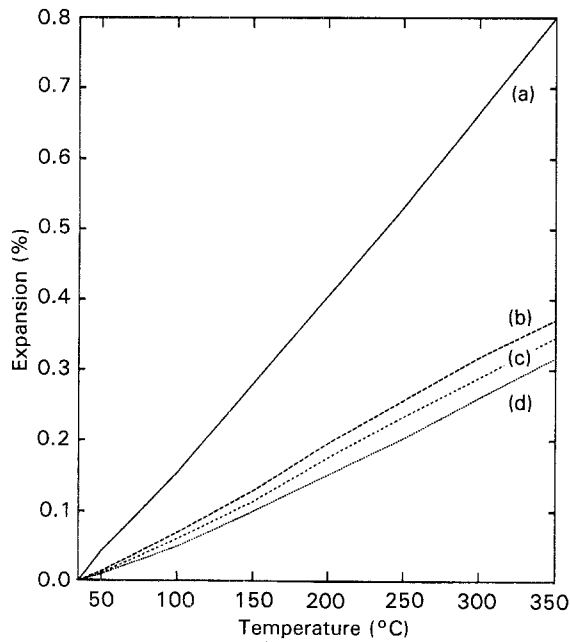

Figure 21 Typical curves of fractional expansion versus temperature for aluminium and Al/AlN of various AlN volume fractions in the temperature range 35–350 °C. (a) Al170.1, (b) 55 vol% AlN, (c) 63 vol% AlN, (d) 69 vol% AlN.

TABLE IX The mean coefficient of thermal expansion[a] of AlN composites in various temperature ranges

Al matrix	Vol%	CTE $(10^{-6}\,°C^{-1})$			
		35–100 °C	35–200 °C	35–300 °C	35–350 °C
170.1	0	22.71 (0.35)	24.26 (0.21)	24.81 (0.18)	25.15 (0.36)
	55.0	9.81 (0.21)	10.77 (0.10)	11.75 (0.12)	11.81 (0.33)
	58.6	9.76 (0.19)	10.60 (0.04)	11.55 (0.04)	11.71 (0.40)
	61.5	9.38 (0.29)	10.15 (0.37)	10.85 (0.01)	11.54 (0.31)
	63.0	8.92 (0.19)	9.88 (0.04)	10.54 (0.05)	11.13 (0.41)
	69.0	8.48 (0.14)	9.60 (0.03)	10.02 (0.09)	10.30 (0.06)
6061	0	22.02 (0.19)	23.76 (0.53)	24.36 (0.11)	24.69 (0.27)
	54.6	10.16 (0.47)	11.14 (0.11)	12.21 (0.20)	12.44 (0.23)
	62.0	8.32 (0.08)	9.90 (0.18)	10.40 (0.20)	10.57 (0.15)
413.1	0	19.20 (0.45)	20.43 (0.12)	21.48 (0.30)	22.66 (0.15)
	57.9	7.87 (0.57)	8.90 (0.19)	9.53 (0.03)	9.79 (0.04)
Al–20Si–5Mg	0	16.63 (1.10)	17.84 (0.74)	19.69 (0.38)	20.47 (0.08)
	57.9	7.10 (0.09)	8.18 (0.55)	9.08 (0.35)	9.52 (0.18)
Al–40Si–1Mg	0	14.40 (0.26)	15.61 (0.10)	15.78 (0.22)	15.60 (0.30)
	54.4	6.74 (0.20)	7.90 (0.32)	8.62 (0.40)	8.85 (0.56)
Al–40Si–1Mg (refined)[b]	0	12.43 (0.21)	13.28 (0.33)	14.09 (0.23)	13.94 (0.28)
	55.0	6.41 (0.50)	7.75 (0.34)	8.21 (0.40)	8.56 (0.61)

[a] Standard deviation shown in parentheses.
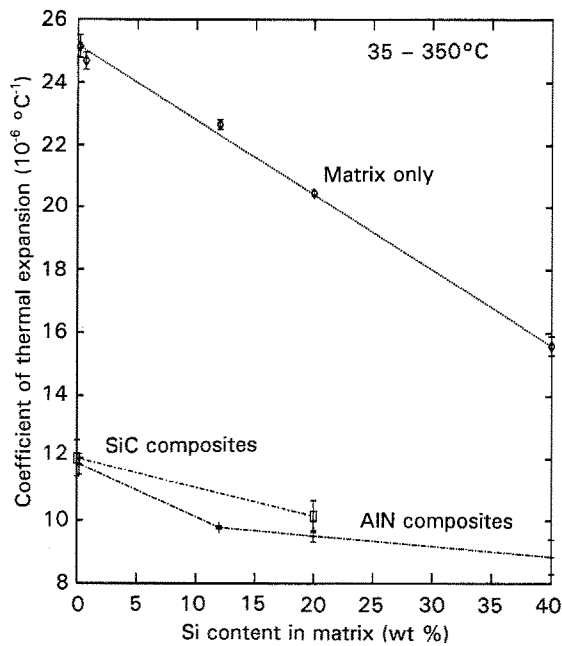[b] Refined with phosphorus.

Figure 22 The CTE of the matrices, the AlN composites and the SiC composites as functions of the matrix silicon content. The AlN composites include Al/AlN (55 vol% AlN), 413.1/AlN (57.9 vol% AlN), Al–20Si–5Mg/AlN (57.9 vol% AlN) and Al–40Si–1Mg/AlN (54.4 vol% AlN). The SiC composites include Al/SiC (55 vol% SiC) and Al–20Si–5Mg/SiC (55 vol% AlN).
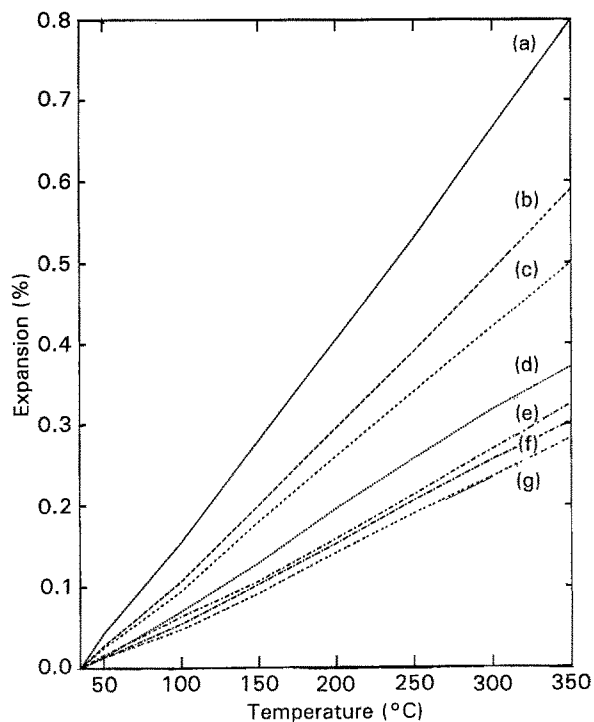

Figure 23 The typical curves of fractional expansion versus temperature of various matrices and the resulting AlN and SiC composites. Al–20Si–5Mg/SiC had a larger CTE compared to Al–20Si–5Mg/AlN. (a) A1170.1, (b) Al–20Si–5Mg, (c) Al–40Si–1Mg, (d) Al/AlN, (e) Al–20Si–5Mg/SiC, (f) Al–20Si–5Mg/AlN, (g) Al–40Si–1Mg/AlN.

calculated values based on Kerner's model [24]. However at 35–350 °C, the measured values were between the predictions of the Rule of Mixtures (ROM) and Kerner's model. The measured CTE values for both
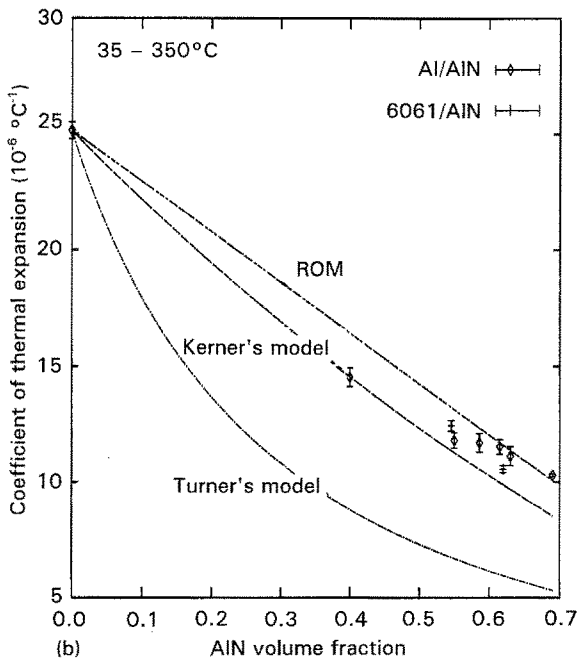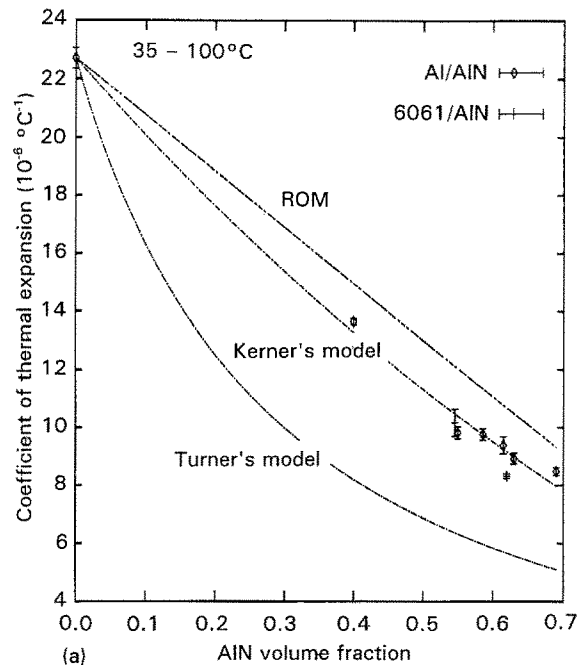

Figure 24 Comparison of the measured CTE values of Al/AlN and 6061/AlN with the theoretical values (ROM, Kerner's, Turner's), as functions of the AlN volume fraction.

temperature ranges were far from the calculated values based on Turner's model [25].

2.2.5. High-temperature mechanical deformation

The resistance to compressive deformation at a constant temperature of 525 °C and a constant compressive stress of 0.2 MPa was measured on Al/AlN (59 vol% AlN) and Al/SiC (60 vol% SiC) which had been first heated from room temperature to 525 °C at a heating rate of 5 °C min^{-1}. Fig. 25 shows the fractional expansion, as measured by using a thermal mechanical analyser (Perkin–Elmer TMA7), during the initial period of linear temperature increase and

the subsequent period (100 min long) of constant temperature (525 °C). The compressive load of 0.2 MPa was applied in the direction of the measured sample dimension throughout both periods. Fig. 25 shows that Al/AlN exhibited a more linear expansion curve than Al/SiC during the initial period of linear temperature increase. During the subsequent period of constant temperature, Al/AlN expanded, whereas Al/SiC shrank. The expansion of Al/AlN is due to the thermal expansion toward the equilibrium dimension at 525 °C, because the sample was not heated infinitely slowly from room temperature to 525 °C. The shrinkage of Al/SiC is due to the softening of the matrix and the resulting deformation under the applied compressive stress. The matrix softening is more severe in Al/SiC than Al/AlN because of the reaction between aluminium and SiC and the resulting Al–Si alloy (which has a lower melting temperature than aluminium) in the matrix. The non-linear expansion curve of Al/SiC in the initial period of linear temperature increase was such that the expansion of Al/SiC was less than Al/AlN at low temperatures and greater than Al/AlN at high temperatures. This non-linear behaviour of Al/SiC is again attributed to the reaction between aluminium and SiC and the resulting Al–Si alloy in the matrix. This reaction was more severe at high temperatures.

The 525 °C compressive testing showed that Al/AlN was more resistant to high-temperature mechanical deformation than Al/SiC.

3. Discussion

This work showed that AlN particles are better than SiC or Al_2O_3 particles for providing aluminium–matrix composites of high strength, high ductility and good high-temperature resistance.

The superior effect of AlN compared to SiC is due to the fact that AlN does not react with aluminium whereas SiC does. The reaction of SiC with aluminium degrades the bonding between SiC and aluminium, so that both the strength and ductility decrease significantly after heating at 600 °C. Particle decohesion was observed from the Al/SiC fracture surface, but not from the Al/AlN counterpart. Moreover, fewer micro-dimples were observed for Al/SiC than Al/AlN.

The superior effect of AlN compared to Al_2O_3 is due to the greater ease of infiltration of AlN than Al_2O_3, which resulted from the difference in preform morphology and probably in wettability by liquid aluminium [26]. The same method of preform preparation was used for AlN, SiC and Al_2O_3. Fig. 26 shows scanning electron micrographs of the centres of SiC and Al_2O_3 preforms. No binder was observed distinctly in either SiC or Al_2O_3 preforms. Like the AlN preform (as shown in Fig. 4), the SiC preform exhibited no particle clustering. In contrast, the Al_2O_3 preform showed particle clustering throughout the preform, such that fine particles were attached to larger particles (Fig. 26b). The clustering of the Al_2O_3 particles was found to occur even in the absence of a binder, as shown in Fig. 1c. The Al_2O_3 particle
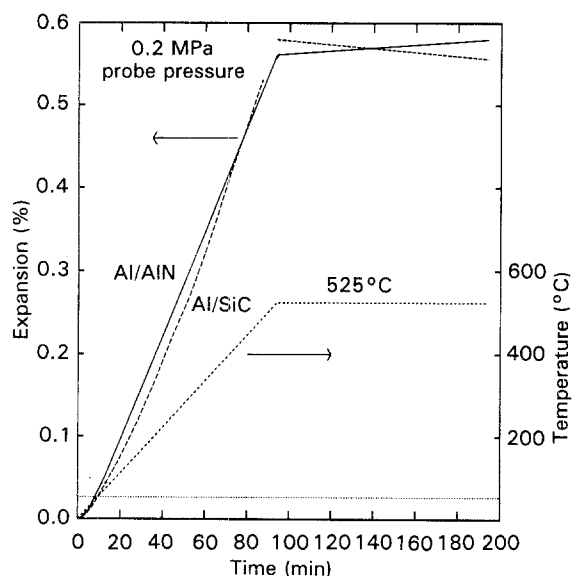
Figure 25 Fractional expansion versus time, and temperature versus time during the initial period of linear temperature increase from room temperature to 525 °C and the subsequent period of constant temperature (525 °C). A compressive stress of 0.2 MPa was applied during both periods. The data shown are for Al/AlN (59 vol% AlN) and Al/SiC (60 vol% SiC).
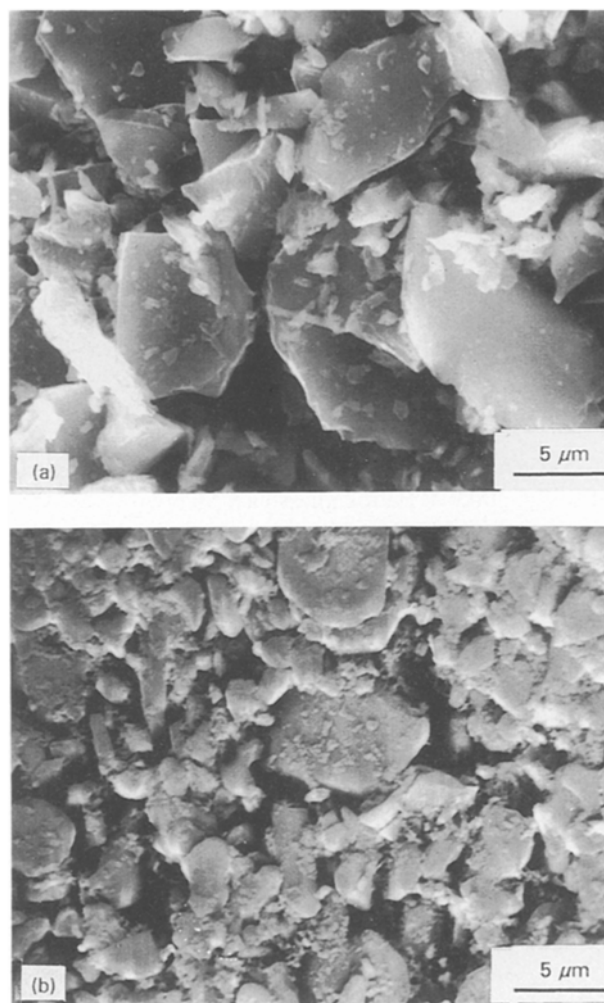
Figure 26 Scanning electron micrographs of (a) SiC and (b) Al_2O_3 preforms.

6195

clustering made it difficult for the Al_2O_3 to be completely infiltrated, thus resulting in a high porosity and inferior mechanical properties of Al/Al_2O_3 compared to Al/AlN and Al/SiC.

The choice of the aluminium alloy for the matrix of Al/AlN is a major factor that affects the strength and ductility of the composite. Table X shows the strength and ductility of AlN composites in relation to the matrix ductility for the aluminium matrices of 170.1, 6061, Al–5Mg, 413.1 and Al–20Si–5Mg. Except for 6061, which was heat-treatable (precipitate hardening), the rest of the matrices were not heat treatable. Only the composite in the as-cast (F temper) condition was studied. In general, the strength of a composite increases with increasing reinforcement volume fraction up to 30 vol%, as long as the composite displays sufficient ductility to reach the maximum strength. At a high reinforcement content exceeding 30 vol%, the rate of strength increase tends to decrease because the composite fails while still in the precipitously rising portion of the stress–strain curve. When the matrix of the composite does not have the adequate local ductility to redistribute the very high regional internal stress, the composite fractures before reaching the normal ultimate strength. This is the case for the aluminium matrices of low ductility. As shown in Table X, both Al–12Si and Al–20Si–5Mg matrices exhibited ductility less than 3.5% (in contrast to the other matrices in Table X) and resulted in AlN composites of low ductility and low tensile strength. In contrast, the aluminium matrices with higher ductility, like 170.1 (aluminium), 6061 (Al–1.0Mg–0.7Si) and Al–5Mg, resulted in higher ductility and tensile strength in the corresponding composites at similar AlN volume fractions. This means that the choice of a ductile aluminium matrix is a key factor for attaining a high ultimate tensile strength in AlN composites at the high AlN volume fraction.

Among AlN composites having a similar volume fraction of AlN, 6061/AlN exhibited the highest strength (e.g. 491.1 MPa for an as-cast 58.1 vol% 6061/AlN composite, Table IV), followed by Al–5Mg/AlN (e.g. 465.2 MPa for an as-cast 60 vol% Al–5Mg/AlN composite, Fig. 12a and then pure Al/AlN (e.g. 300.9 MPa for an as-cast 58.6 vol% Al/AlN composite, Table III). It may be attributed to the higher matrix strength and the stronger interface in

the former two AlN composites due to the presence of magnesium and its resulting precipitates. The increase in flow stress of the former two composites presumably reflects the incremental effects of dislocation interaction with the aluminium alloy's precipitates. From the Al–Mg phase diagram, Al–5Mg is not heat treatable, but can be dispersion strengthened upon slow cooling. The Mg_2Si precipitate might be produced in 6061/AlN upon slow cooling in the presence of ample AlN, even without artificial ageing. The greater dislocation density in the former two composites caused these two composites higher flow stresses for deformation, thus resulting in higher tensile strengths for these composites. On the other hand, AlN composites of all three matrices exhibited a similar ductility of about 1% and the same fracture morphology.

Based on the H–S model, the calculated moduli of 6061/AlN (58.1 vol%) and Al–5Mg/AlN (60.0 vol%) are 157.9 and 162.7 GPa, respectively. (The moduli of both matrices are 70.2 GPa.) That the calculated moduli and the measured moduli in Fig. 12b and Table V are similar indicates the validity of the H–S model for describing the modulus of Al/AlN with various aluminium matrices.

The modulus of Al/AlN is independent of heat treatments (whether T6 or heating at 600 °C for 10 or 20 days). This implies that precipitation strengthening or interface degradation, if any, will not change the modulus of the composite. The modulus of a sound AlN composite is also independent of the infiltration pressure used during fabrication.

The absence of an interfacial reaction between aluminium and AlN allowed Al/AlN to have a higher resistance to thermal degradation compared to Al/SiC. As shown in Fig. 13, Al/AlN (62 vol%) annealed at 600 °C for 480 h exhibited a 10% reduction of the room-temperature tensile strength, whereas Al/SiC (55 vol%) similarly heat treated showed a 26% reduction of the room-temperature tensile strength. The superior high-temperature resistance of Al/AlN compared to Al/SiC is also indicated by compressive testing (deformation versus time) at a constant temperature of 525 °C and a constant stress of 0.2 MPa. Regardless of interfacial reactions, the reduction in strength of the extensively annealed Al/AlN was expected due to thermally activated flow processes and

TABLE X The effect of matrix ductility on the tensile strength of AlN composites

AlN vol%	Al matrix		Composite	
	Major alloying element(s)	Ductility (%)[a]	Strength (MPa)[b]	Ductility (%)
58.6		40	300.9 (25.2)	1.0
61.5		40	385.8 (23.9)	1.1
60.0	5 Mg	10–35	465.2 (10.7)	1.0
58.1	1.0 Mg, 0.7 Si	12–25	491.1 (21.0)	1.0
57.9	12 Si	3.5	233.1 (25.3)	0.3
57.9	20 Si, 5 Mg	< 3	225.4 (10.8)	0.2

[a] From [27].
[b] Standard deviation shown in parentheses.

void (or defects) nucleation and growth at 600 °C. Both would cause degradation in the Al–AlN interface and/or thermal damage in AlN itself. The little difference in the fracture surface morphology of Al/AlN before and after the heat treatment is consistent with the small effect of the heating on the tensile strength of Al/AlN. On the other hand, the ductility of Al/AlN decreased and the size of the AlN particle cleavage facets increased with increasing heating time at 600 °C.

Although Al_2O_3 is not reactive with aluminium, Al/Al_2O_3 exhibited the largest strength and ductility reduction due to the heating at 600 °C. It is due to the fact that, under the same fabrication conditions, the Al/Al_2O_3 composite was not well-infiltrated due to the high resistance to wetting between aluminium and Al_2O_3. The small non-infiltrated Al_2O_3 clusters in the composite caused Al/Al_2O_3 to be more prone to thermal degradation compared to Al/AlN or Al/SiC.

The Al/SiC (55.0 vol%) in this work exhibited a tensile strength of about 150 MPa at 400 °C, which was 30 MPa higher than that of 2124/SiC (20 wt %), also at 400 °C [10]. It had been observed [9] that 1100/SiC/20%, 2124/SiC/20% and unreinforced 2124 reached a nearly identical strength of 70 MPa at 400 °C. The difference between the present study and previous reports [9, 10] may be ascribed to the higher volume fraction of reinforcement used in this work. The improvement of the mechanical properties of metal–matrix composites depends on the reinforcement strength, the matrix shear strength and how well the matrix can transfer load to the reinforcement via a strong interface. Assuming a perfect interface, a general equation relating the maximum stress transferred from the matrix to a fibre can be expressed as

$$\sigma_f = 2\tau_m l/d \qquad (1)$$

where σ_f is the fibre stress, τ_m is the matrix shear strength, d is the fibre diameter and l is the fibre length.

As the matrix shear strength is reduced at elevated temperatures, less load can be transferred to the fibres, resulting in a lower composite tensile strength. This model holds true for most composites in the range of 15–30 vol%. As a higher volume fraction of fine particles causes a smaller interparticle spacing, a dislocation model related to the plastic strain generated near particles by mismatch in thermal expansion coefficients would lead to an Orowan-type relation. Hence, more resistance to plastic deformation in the composite would be obtained at 400 °C compared to what is expected from Equation 1, though the interfacial shear strength, which can be assumed to be the yielding shear stress of the matrix, decreases with increasing temperature.

Although the addition of 7 wt % or more silicon in the matrix could prevent the Al–SiC reaction during the fabrication of Al/SiC [28], it also decreased the matrix ductility which, in turn, decreased the tensile strength of the resulting composites. As shown in Table VIII, both Al–20Si–5Mg/AlN and Al–20Si–5Mg/SiC exhibited similar strength, modulus and ductility before and after heat treatment at 500 °C for 480 h. This indicates that the SiC composite attained

similar mechanical properties as the AlN composite provided that little or no Al–SiC interfacial reaction occurred. The Al–SiC reaction was not aggravated during heating at 500 °C for 480 h, if Al–20Si–5Mg instead of aluminium was used as the matrix. Because a ductile matrix is critical for obtaining high strength in a composite having a high volume fraction of the reinforcement, a matrix like pure aluminium with ductility up to 50% is attractive, even though, in this case, the Al–SiC reaction cannot be avoided and results in mechanical property degradation at elevated temperatures. An Al–Si alloy matrix of lower ductility than pure aluminium can avoid the Al–SiC reaction, but it causes significant decreases in the strength and ductility of the composite, even in the as-cast state.

The Al/AlN (58.6%) composite had higher strengths at 300 and 400 °C than the Al/SiC (55.0%) composite. This could be ascribed to the brittle interface formed in Al/SiC and the fact that a fraction of SiC was reacted away.

At 400 °C, less cleavage of the reinforcement particles was observed due to the softened matrix. Very high local stresses within the SiC or AlN particles need to be achieved before particle fracture occurs. This can only be obtained in the presence of a strong matrix.

The CTE of the aluminium–matrix composites can be decreased by increasing the volume fraction of the reinforcement and increasing the silicon content of the aluminium matrix. Although the range of filler volume fraction was narrow, the CTE values of Al/AlN were found to lie in between the predictions of the Rule of Mixtures and Kerner's model. The CTE of the matrix decreased linearly with increasing silicon content up to 40 wt %, whereas the CTE of both AlN and SiC composites decreased significantly with increasing silicon content up to about 12 wt % only. It was also found that the addition of a phosphorus refiner decreased the CTE of Al–40Si–1Mg from 14.40×10^{-6} to $12.43 \times 10^{-6}\,^{\circ}C^{-1}$, but decreased the CTE of the resulting Al–40Si–1Mg/AlN composite only slightly. Metallography showed that the morphology of Al–40Si–1Mg/AlN was the same before and after the use of the refiner.

4. Conclusion

1. Al/AlN had a higher tensile strength and a higher tensile ductility than Al/SiC of a similar filler volume fraction at 400 °C or at room temperature after heating at 600 °C. Al/Al_2O_3 had an even lower strength and a smaller ductility than Al/SiC of a similar filler volume fraction at room temperature after heating at 600 °C.

2. Al/AlN had greater resistance to compressive deformation at 525 °C than Al/SiC.

3. The curve of the fractional expansion versus temperature (from room temperature to 525 °C) was linear for Al/AlN, but concave upward for Al/SiC, so that the fractional expansion was larger for Al/AlN than Al/SiC at low temperatures (below 450 °C for a heating rate of 5 °C min^{-1}) and smaller for Al/AlN than Al/SiC at high temperatures (above 450 °C for a heating rate of 5 °C min^{-1}).

6197

4. AlN in the amount of 69 vol% decreased the CTE of aluminium from 25.2×10^{-6} to $10.3 \times 10^{-6} \,^{\circ}C^{-1}$. The CTE decrease agrees quite well with that predicted by the Rule of Mixtures at high filler volume fractions. The addition of 40 wt % Si into the aluminium matrix decreased the CTE of Al–40Si–1Mg/AlN (57 vol% AlN) to $6.41 \times 10^{-6} \,^{\circ}C^{-1}$ at 35–100 °C and $8.85 \times 10^{-6} \,^{\circ}C^{-1}$ at 35–350 °C.

5. An infiltration pressure of up to 6000 p.s.i. (41 MPa) was needed for the fabrication of a sound Al/AlN composite. The resulting porosity was less than 1.4%. The Al–5Mg alloy as the matrix required less infiltration pressure than the case of pure aluminium as the matrix. Magnesium probably caused an increase in the wettability of AlN, thereby resulting in stronger bonding at the interface.

6. For the 6061 Al alloy as the matrix, the T6 heat treatment strengthened the composite containing 58 vol % AlN by only 5%, compared to 107% for the matrix by itself. However, it gave the highest tensile strength among the three matrices used, i.e. pure aluminium, Al–5Mg and 6061.

7. The filler–matrix interface was more brittle in Al/SiC than in Al/AlN. The unreactive nature of AlN with aluminium resulted in a more ductile interface, as shown by a combination of locally ductile and brittle fracture morphology for Al/AlN. In contrast, the formation of Al_4C_3 and silicon due to the reaction between aluminium and SiC deteriorated both the SiC particles and the interface. Although Al_2O_3 is not reactive with aluminium, insufficient infiltration of Al_2O_3 resulted in the lowest strength and ductility among Al/Al_2O_3, Al/SiC and Al/AlN.

8. The addition of AlN or Al_2O_3 increased the modulus of aluminium in accordance with the model of Hashin and Shtrikman (H–S), but the SiC addition increased the modulus of aluminium by an amount that exceeded the prediction of H–S. This is due to the large aspect ratio of the SiC particles.

References

1. ALAN L. GEIGER and MICHAEL JACKSON, *Adv. Mater. Proc.* **136**(1) (1989) 23.
2. ALAN L. GEIGER, private communications.
3. M. K. AGHAJANIAN, J. T. BURKE, D. R. WHITE and A. S. NAGELBURG, *SAMPE Q.* **20** (4) (1989) 43.
4. C. TOY and W. D. SCOTT, *J. Am. Ceram. Soc.* **73**(1) (1990) 97.
5. A. SAKOMOTO, H. HASEGAWA and Y. MINODA, in "Proceedings ICCM/5", edited by W. C. Harrigan Jnr., J. Strife and A. K. Dhingra (Metallurgical Society of AIME, New York, 1985) pp. 705–7.
6. D. L. McDANELS and C. A. HOFFMAN, NASA technical paper 2302 (1984).
7. W. L. PHILLIPS, in "Proceedings ICCM/2", edited by B. R. Noton (Metallurgical Society of AIME, Warrendale, PA, 1978) pp. 567–76.
8. C. S. LIN, SAE Technical Paper Series 902013, Aerospace Technology Conference and Exposition, Long Beach, CA, 1–4 October 1990 (SAE, Warrendale, PA, 1990).
9. R. D. SCHUELLER and F. E. WAWNER, *Compos. Sci. Technol.* **40** (1991) 213.
10. S. F. CORBIN and D. S. WILKINSON, in "Proceedings of Ceramic and Metal Matrix Composites", Proceedings of the International Symposium on Advanced Processing of Ceramic and Metal Matrix Composites, edited by H. Mostachaci (1989).
11. Advanced Composite Materials Corp., data sheet.
12. A. SAKOMOTO, H. HASEGAWA and Y. MINODA, in "Proceedings ICCM/5", edited by W. C. Harrigan Jnr., J. Strife and A. K. Dhingra (Metallurgical Society of AIME, New York, 1985) pp. 699–705.
13. W. POLLOCK and F. E. WAWNER, in "12th Conference on Composite Materials and Structures", Cocoa Beach, FL, 20–22 January, 1988.
14. L. ACKERMANN, J. CHARBONNIER, G. DESPLANCHES and H. KOSLOWSKI, in "Proceedings ICCM/5", edited by W. C. Harrigan, J. Strife and A. K. Dhingra (Metallurgical Society of AIME, New York, 1985) pp. 687–98.
15. J. DINWOODIE, E. MOORE, C. LANGMAN and W. SYMES, *ibid.*, pp. 671–85.
16. A. BANERJI and P. K. ROHATGI, *J. Mater. Sci.* **17** (1982) 335.
17. J. A. CORNIE, A. MORTENSEN and M. C. FLEMINGS, in "Proceedings ICCM/6", edited by F. L. Matthews, N. C. R. Buskell, J. M. Hodginson and J. Morton, Elsevier, Vol. 2 (1987) pp. 2297–319.
18. JENG-MAW CHIOU and D. D. L. CHUNG, *J. Mater. Sci.* **28** (1993) 1435.
19. Idem, *ibid.* **28** (1993) 1447.
20. Idem, *ibid.* **28** (1993) 1471.
21. S.-Y. OH, J. A. CORNIE and K. C. RUSSELL, *Met. Trans.* **20A** (1989) 527.
22. Z. HASHIN and SHTRIKMAN, *J. Mech. Phys. Solids* **11** (1963) 127.
23. SHY-WEN LAI and D. D. L. CHUNG, *J. Mater. Sci.*, **29** (1994) 2998.
24. E. H. KERNER, *Proc. Phys. Soc.* **69** (1963) 802.
25. P. S. TURNER, *J. Res. NBS* **37** (1946) 239.
26. M. G. NICHOLAS, D. A. MORTIMER, L. M. JONES and R. M. CRISPIN, *J. Mater. Sci.* **25** (1990) 2679.
27. J. E. HATCH (ed.), " Aluminium: Properties and Physical Metallurgy" (ASM, Metals Park, OH, 1984).
28. D. J. LLOYD, H. LAGACE, A. McLEOD and P. L. MORRIS, *Mater. Sci. Eng.* **A107** (1989) 73.